Finite Deformation Analysis of Crack Tip Opening in Elastic-Plastic Materials and Implications for Fracture Initiation

R. M. McMeeking

Division of Engineering

Brown University

Providence, R. I. 02912

May 1976

DISCLAIMER

SUMMARY

Analyses of the stress and strain fields around smoothly blunting crack tips in both non-hardening and hardening elastic-plastic materials, under contained plane strain yielding and subject to mode I opening loads, have been carried out by a finite element method suitably formulated to admit large geometry changes. The results include the crack tip shape and near-tip deformation field, and the crack tip opening displacement has been related to a parameter of the applied load, the J-integral. The hydrostatic stresses near the crack tip are limited due to the lack of constraint on the blunted tip, limiting achievable stress levels except in a very small region around the crack tip in power law hardening materials. The J-integral is found to be path independent except very close to the crack tip in the region affected by the blunted tip. Models for fracture are discussed in the light of these results including one based on the growth of voids. The rate of void growth near the tip in hardening materials seems to be little different from the rate in non-hardening materials when measured in terms of crack tip opening displacement, which leads to a prediction of higher toughness in hardening materials. It is suggested that improvement of this model would follow from better understanding of void-void and void-crack coalescence and void nucleation, and some criteria and models for these are discussed. The implications of the finite element results for fracture criteria based on critical stress, strain or both is discussed with respect to transition of fracture mode and the angle of initial crack growth. Localization of flow is discussed as a possible fracture model and as a model for void-crack coalescence.

1. INTRODUCTION

When an elastic-plastic body with a sharp crack is subject to a monotonically increasing load of the mode I type (i.e., tensile opening), blunting of the tip by intense straining will occur until some mechanism of crack extension gradually or abruptly takes over. Study of slip line configurations around crack or notch tips such as shown by McCLINTOCK (1971, pp. 158-159) and RICE and JOHNSON (1970) (henceforth referred to as RJ), leads one to conclude that two types of blunting are possible. The first type is vertex blunting,where localized shearing singularities on the tip give rise to a blunted tip shape of two or more vertices connected by straight segments,and the second type is where blunting gives rise to a smoothly curved tip shape. The fact that both types occur is confirmed by an observation by McCLINTOCK (1971, p. 159) of the first type in a specimen of 1100 aluminum with a groove with a flat tip,and an observation by RAWAL and GURLAND (1976) of the second type,which arose from a pre-fatigued crack in spheroidized steel. The type of blunting which arises in a specific case may depend on considerations of strain hardening and stability (pp. 158-160, McCLINTOCK, 1971). However the smooth blunting case, which may be viewed as the limiting case of a very large number of vertices on the blunted tip, has features of some generality,and has the advantage of being amenable to solution by an ordinary, plane strain continuum, finite element method suitable for large deformations such as that of McMEEKING and RICE (1975). The smooth blunting case was solved for near-tip stresses and deformations by that method for both hardening and non-hardening materials with boundary conditions simulating the situation of plastic yielding contained near the tip of the crack.

In their work RJ noted that the severe stretching ahead of the crack tip can be predicted only by an analysis of crack blunting such as they carried out for non-hardening materials. Studies, such as those of RICE (1968), RICE and ROSENGREN (1968), HUTCHINSON (1968), RICE and TRACEY (1973) and TRACEY (1973, 1976), ignoring large geometry change but based on strain singularities at the tip, predict only intense shearing above and below the tip and a state of triaxial stress immediately ahead of the crack tip. The blunting analysis, however, reveals that this stress triaxiality cannot be maintained at the blunted surface of the crack. Thus an understanding of some phenomena observed to be associated with rupture may have to be based on a large geometry change analysis of the near tip behavior, (e.g., straight ahead crack growth; angled crack growth; plastic void growth, which is known to be heavily influenced by the hydrostatic component of stress as shown by McCLINTOCK (1968a) and RICE and TRACEY (1969)). This point seems to be confirmed by observations by RJ and RICE (1973), based on metallographic studies of ductile fracture by BIRKLE, WEI and PELLISSIER (1966) and PELLISSIER (1968) in high strength steel and VAN STONE, MERCHANT and LOW (1974) in aluminum alloys, all of which indicate that the crack tip opening displacement at fracture in small scale yielding compares in size with typical distances between particles which seem to nucleate voids playing a primary role in fracture. Study of the fracture surfaces near the transition region between the crack and the fast fracture area in these materials indicates that events, such as nucleation of smaller voids, take place near the tip on a size scale much smaller than a crack tip opening displacement, and in an area certainly affected by blunting. On the other hand, if the critical event at fracture is based on a size scale much larger than a crack tip opening displacement, then blunting will play little or no role. Such a case arises for a model developed by RITCHIE, KNOTT and RICE

(1973) for predicting slip nucleated cleavage in mild steel, based on a requirement that a critical stress for cleavage be achieved over some distance measured from the crack tip. It turns out that the best correlation occurs when the critical distance coincides with two grain sizes, and at the low temperature end of the data this size is about 50 times the crack tip opening displacement at fracture.

After a description of the solution procedure and the results of the finite element analysis of smooth crack tip blunting presented in the next two sections, brief comments are made concerning vertex blunting. Then the results of a void growth model for ductile fracture already developed by RJ are discussed, especially concerning what it implies for hardening materials and how it might be improved by better modeling of void-crack coalescence and void nucleation. In addition, fracture criteria based on achieving a critical stress, a critical strain or a combination of critical stress and strain are discussed in relation to the stresses and plastic strains around the blunted crack tip. In addition, localization of flow in narrow bands is discussed both as a model for ductile fracture and for the coalescence of voids.

2. PLANE STRAIN NOTCH BLUNTING SOLUTIONS BY FINITE ELEMENTS

It was intended that the finite element calculations should model the blunting of an initially sharp crack, but the initial crack tip singular behavior rules out any simple method of accurately starting such a computation. To overcome this problem, the calculations were carried out for a notch with a semi-circular tip in the undeformed configuration. It was expected that a steady state solution for contained yielding, largely independent of original notch geometry, would arise after a sufficient amount of load was applied. Here and henceforth the phrase "steady state solution" for the blunting of an initially sharp crack will be used to mean a continuous series of evolving, self-similar states, having the property that when displacements and lengths are normalized by a loading parameter $K^2/\sigma_o E$, a solution unchanging in time is obtained. In the loading parameter, K is the strength of the elastic crack tip singularity which would arise from the applied loads if the material was linear elastic (IRWIN, 1960), σ_o is the yield strength in tension of the actual material and E is Young's modulus. The term $K^2/\sigma_o E$ has dimensions of length, and the crack tip opening displacement may be used instead as the normalizing parameter, since, on dimensional grounds, the crack tip opening displacement is equal to $K^2/\sigma_o E$ times a function of dimensionless groups of material properties.

The expectation that a steady state solution would arise was based on the work of RJ, who found that the shape of the tip of the notch, smoothly blunted by loads representing small scale yielding, could be obtained at all times from the shape of a sharp crack blunted by the same loads by adding to the sharp crack blunted shape in a certain constant way the original notch shape. This procedure is equivalent to the superposition in Henky

nets discussed by HILL (1967). As the total notch width grows to several times the original notch width, the difference between the blunted notch shape and the shape of a sharp crack blunted by the same boundary conditions becomes negligible, and so the notch results may then be used as a good approximation for the blunting of a sharp crack. The results of RJ were derived by the slip line method (HILL, 1950, pp. 128-160), and are therefore strictly applicable only to non-hardening materials. However, the steady state solution for the sharp crack case in RJ does not arise as a consequence of the lack of hardening, but rather because the crack tip opening displacement is the only length of significance in the near tip field in small scale yielding, and so all distances in the solution scale with crack tip opening displacement. This feature will carry over to hardening materials, and so the results for notch blunting should achieve a steady state which can be interpreted appropriately for initially sharp cracks. The interpretation of the results on the blunted surface for power law hardening materials requires some care, since blunting from sharp cracks involves infinite plastic strains and consequently infinite flow stress on the blunted surface, while blunting from a notch will cause only large but finite strains.

2.1 The finite element mesh

To provide the information required in the solution, the mesh must contain near the initial notch tip elements which are much smaller in typical dimension than the radius of the original notch tip. On the other hand, the problem geometry must be sufficiently large compared to the notch tip radius so that boundary conditions may be applied to represent the situation of small scale yielding around a crack tip. This mandates a mesh with a dramatic refinement near the tip in order to keep the mesh size at an

acceptable level. Another problem is that the solution should still have accuracy after blunting, say, to five times the original crack tip opening displacement,after which the near tip elements would have experienced a change in a particular dimension of order five times that dimension. This difficulty was overcome by choosing the original near tip element shape so that,as an element deformed,it would experience an extensional strain along the side originally short and a shortening strain along the side originally long. Then the shape of a highly strained element throughout its loading history would be kept to a sequence of shapes and sizes considered acceptable for the purposes of calculating gradients of stress and plastic strain.

A mesh used is shown in fig. 1 in its undeformed configuration. This mesh, designated mesh I, contains 316 nodes and 260 plane strain isoparametric quadrilateral elements with four stations for the integration of stiffness (ZIENKIEWICZ, 1971 pp. 129-153). Another mesh, mesh II, was used with an extra ring of elements around the outer radius of mesh I. Mesh II had 329 nodes and 272 elements.

2.2 Boundary conditions for notch blunting

The notch blunting solution for small scale yielding was achieved by applying traction free boundary conditions on the notch surface,and displacement boundary conditions elsewhere imposing an asymptotic dependence on the mode I elastic crack tip singular field of IRWIN (1960). This was done indirectly by actually using in a manner described below,displacements calculated from the small strain finite element results of RICE and TRACEY (1973) and TRACEY (1973, 1976), who accounted for phenomena occurring at the crack tip due to plasticity in both non-hardening and hardening

materials by using special crack tip elements. These imposed the characteristic near tip displacement behavior derived by HRR. The conditions applied at the circular boundaries of their meshes were the displacements of the elastic singular field,so that crack tip plasticity is accounted for in the manner of a boundary layer formulation as discussed by RICE (1967a, 1968). In these finite element calculations, steady state solutions develop and persist as long as the plastic zones lie well within the outer boundaries of the mesh. These steady state solutions have the feature discussed above that displacements and characteristic distances scale with crack tip opening displacement. This result may be stated as

$$\begin{aligned} E\underset{\sim}{u}(R,\phi)/(\sigma_o \delta_t) &= E'\underset{\sim}{u}'(R', \phi)/(\sigma_o' \delta_t') \\ R/\delta_t &= R'/\delta_t' \quad , \end{aligned} \tag{1}$$

where $\underset{\sim}{u}'$ is the steady state displacement at position R',ϕ in polar coordinates with origin at the crack tip,at the time when the crack tip opening displacement is δ_t' in a material of Young's modulus E' and tensile yield stress σ_o',and $\underset{\sim}{u}$ is the steady state displacement at R,ϕ for crack tip opening displacement δ_t',Young's modulus E, tensile yield stress σ_o and all other material properties identical to those in the prime (') material. The factors E/σ_o and E'/σ_o' enter (1) in the way they do because universal solutions to problems formulated with conventional small strain assumptions exist and are phrased in terms of $E\underset{\sim}{u}/\sigma_o$, $\underset{\sim}{\sigma}/\sigma_o$, dimensionless groups of material properties other than σ_o/E and a suitable length measure ($\underset{\sim}{\sigma}$ is the stress tensor).

The displacement history at a fixed point R,ϕ in the unprimed material

can thus be calculated from the displacements in the primed material steady state solution at some fixed crack tip opening displacement δ_t' through

$$\underset{\sim}{u}(R,\phi) = \left(E'\sigma_o R/(E\sigma_o' R')\right) \underset{\sim}{u}'(R',\phi) \quad , \tag{2}$$

where R' is taken from ∞ towards zero to develop the history. When R' exceeds the radius of the mesh of finite elements used in RICE and TRACEY (1973) and TRACEY (1973, 1976), the displacements $\underset{\sim}{u}'$ are interpreted as the elastic crack tip singular displacements. This history of displacements can thus serve as the sequence of conditions applied to the boundary of the finite element mesh used for the blunting calculations, with R the outer radius of that mesh. As long as the area affected by the blunting remains small compared to the size of the mesh, the solution will be an accurate boundary layer formulation of the blunting of a notch under conditions of small scale yielding. In view of the comments at the beginning of section 2, no difficulty arises in the boundary layer formulation concept from starting with a finite radius tip, since, when viewed on the size scale of the mesh, its influence is simply a blunting effect introduced initially rather than allowed to rise naturally.

2.3 Finite element formulation and constitutive relations

The up-dated Lagrangian method of McMEEKING and RICE (1975) for large deformation of elastic-plastic materials was used, modified according to appendix 2 of NAGTEGAAL, PARKS and RICE (1974) to free the mesh of artificial constraint. A variational principle, based on a reference state coincident instantaneously with the current state, but derived from the principle of HILL (1958) for arbitrary reference state, is used to formulate the tangent stiffness of a mesh of elements representing

the current shape of the body. The finite element equations are solved in an incremental fashion and the nodes are moved after each incremental solution to represent a new shape of the body. An elastic solution is always carried out first in which one element is permitted to reach yield and then plasticity is allowed to develop gradually. In yielded elements the partial stiffness approach of MARCAL and KING (1967), as modified by RICE and TRACEY (1973) and TRACEY (1973,1976), is used to calculate the stiffness based on a modification of the Prandtl-Reuss equations for isotropically hardening materials (HILL, 1950, pp. 15-39). The constitutive law accounts for rotation of principal deformation axes and is

$$\overset{*}{\tau}_{ij} = \frac{E}{1+\nu}\left[D_{ij} + \frac{\nu}{1-2\nu} D_{kk}\,\delta_{ij} - \frac{3\sigma'_{ij}\sigma'_{k\ell}\,D_{k\ell}\,(\frac{E}{1+\nu})}{2\bar{\sigma}^2(\frac{2}{3}h + \frac{E}{1+\nu})}\right] \tag{3}$$

for plastic loading and

$$\overset{*}{\tau}_{ij} = \frac{E}{1+\nu}\left[D_{ij} + \frac{\nu}{1-2\nu} D_{kk}\,\delta_{ij}\right]$$

for elastic loading or any unloading, where ν is Poisson's ratio, $\underset{\sim}{\sigma}$ is true stress, $\underset{\sim}{\tau}$ is the Kirchhoff stress defined by

$$\underset{\sim}{\tau} = |\underset{\sim}{F}|\,\underset{\sim}{\sigma} \quad ,$$

where $|\underset{\sim}{F}|$ is the ratio of volume in the current state to volume in the reference state, $\underset{\sim}{D}$ is the rate of deformation tensor defined as the symmetric part of the spatial velocity gradient, δ_{ij} is the Kronecker delta,

$$\sigma'_{ij} = \sigma_{ij} - \frac{1}{3}\delta_{ij}\,\sigma_{kk}$$

$$\bar{\sigma}^2 = \frac{3}{2}\sigma'_{ij}\,\sigma'_{ij} \quad ,$$

h is the slope of the uniaxial Kirchhoff stress versus logarithmic plastic strain curve and $\overset{\circ}{}$ denotes the Jaumann or corotational stress rate. In (3), $\overset{*}{\tau}_{ij}$ is chosen rather than $\overset{*}{\sigma}_{ij}$ to generalize Hill's stress rate because the formulation then leads to a symmetric stiffness. The difference between the two generalizations of the law is in any case of order stress divided by elastic modulus compared to unity (McMEEKING and RICE, 1975).

The variational principle mentioned previously is

$$\int_V [\overset{*}{\tau}_{ij}(\underset{\sim}{D})\ \delta D_{ij} - \frac{1}{2}\sigma_{ij}\ \delta(2D_{ik}D_{kj} - v_{k,i}\ v_{k,j})]\ dV = \int_S \dot{f}_i\ \delta v_i dS\ , \tag{4}$$

where V and S are the volume and surface respectively of the body in the current state, $v_{k,i} = \partial v_k/\partial x_i$ where $\underset{\sim}{x}$ is the current position vector of a material point, $\dot{\underset{\sim}{f}}$ is the nominal surface traction rate referred to a reference state which is the current state and δ denotes an arbitrary virtual variation. The modification of NAGTEGAAL et al. (1974) is based on a Lagrange multiplier method, in which element dilation is treated as an independent degree of freedom. It is implemented by changing the definition of $\underset{\sim}{D}$ in the term $\overset{*}{\tau}_{ij}(\underset{\sim}{D})\ \delta D_{ij}$ in (4) in a straightforward manner (NAGTEGAAL et al., 1974, pp. 165-167 and 175-176).

3. RESULTS OF PLANE STRAIN NOTCH TIP BLUNTING BY FINITE ELEMENTS

The calculations were carried out for a material with $\nu = 0.3$, $\sigma_o/E = 1/300$ and a non-hardening ($N = 0$) uniaxial Kirchhoff stress-logarithmic tensile strain curve. In addition calculations for power law hardening materials were processed with $N = 0.1$ and $N = 0.2$ in a uniaxial stress-strain law of the form

$$(\bar{\tau}/\tau_o)^{1/N} = \bar{\tau}/\tau_o + 3G\bar{\epsilon}^p/\tau_o \ , \qquad (5)$$

where $\bar{\tau}^2 = \frac{3}{2}\tau'_{ij}\tau'_{ij}$, τ_o is the tensile yield stress in terms of Kirchhoff stress, G is the shear modulus and $\bar{\epsilon}^p = \int(\frac{2}{3}D^p_{ij}D^p_{ij})^{1/2}dt$, i.e. $\bar{\epsilon}^p$ is the tensile equivalent plastic strain. When the deformation is one of pure shear in the absence of spin in which $D_{12} = D_{21} = \dot{\gamma}/2 = \dot{\gamma}^p/2 + \dot{\gamma}^e/2$, where $\dot{\gamma}^p$ and $\dot{\gamma}^e$ are respectively the plastic and elastic parts of $\dot{\gamma}$, $\bar{\epsilon}^p$ becomes $\gamma^p/\sqrt{3}$ and $\bar{\tau}$ is $\sqrt{3}\,\tau_{12}$. In addition $\tau_{12} = G\gamma^e$ and denoting the Kirchhoff yield stress in shear as $\tau_s = \tau_o/\sqrt{3}$, it follows from (5) that $\tau_{12} = \tau_s(\gamma/\gamma_o)^N$, where $\gamma_o = \tau_s/G$. The calculations for all the above materials used mesh II, while a further calculation with mesh I was undertaken in which $\sigma_o/E = 1/100$, $\nu = 0.3$ and the stress strain curve was non-hardening.

3.1 Blunted tip shapes

If the tip shapes achieved in the notch blunting solutions, shown in figure 2a, were to be drawn so that the intercept of the x-axis with each crack surface coincided, it would be seen that the tip shapes for the four different materials are almost identical. The shapes in figure 2a are for blunting to about five times the original notch width, and they represent a shape that has remained unchanged since the notch had a width

of three times the original notch width.

Differences between the shapes do arise behind the tip, with the non-hardening materials basically having flanks almost parallel to the x-axis and the hardening materials showing an angled flank whose slope becomes steeper with larger values of N. Very far back, outside the plastic zone, the slopes for each case, hardening and non-hardening, approach the same small value. The two non-hardening materials do exhibit different behavior on the flank, with the higher tensile yield strain (σ_o/E) material showing a distinct hump close to the tip. In view of the absence of the hump from the tip shape of the lower yield strain material, it does not appear to be entirely an artifact of element arrangement, although the top of the hump does coincide with the change in element size at the node marked A in figure 2. That node is the material point where the straight flank in the undeformed mesh meets the curved notch surface. A possibility is that there is a real non-uniqueness of blunted notch shape in non-hardening materials, a point of view supported by the non-uniqueness of velocities along the crack surface in slip line solutions for sharply tipped cracks. The actual shape that arises in the blunted notch case could then be influenced by element arrangement.

It is clear in figure 2 that the calculated value for the width of the notch, b, depends on the choice of position chosen to define notch width. However, when points between the deformed position of node A (marked A' in figure 2) and the elastic-plastic boundary on the notch surface are used for defining notch widths, the range of widths involved is small compared to the widths themselves. The arbitrariness of choice in the definition of b is apparent in figure 2, since a choice of a position other than A' for defining b would have changed the tip sizes relative to each other. In

addition,the shapes in figure 2a are drawn as if the point on the x-axis at a distance 2b in front of the intersection of the notch tip and the x-axis in the deformed configuration was stationary.

The blunted tip shape calculated using the slip line method outlined by RJ for the semi-circular notch,when the width of the notch is five times the initial notch width,has been included in figure 2a,and it can be seen to be almost identical to the shapes calculated by finite elements. The slip line pattern around such a notch is shown in the inset of figure 7 and the displacements are calculated relative to the point S which is at a distance about two notch widths ahead of the tip in the deformed configuration. A significant distinction can be seen between the x-displacement of the notches relative to the point two crack widths ahead,and implies a difference in average logarithmic strain of 6×10^{-2} between the crack tip and the point two crack widths ahead when the finite element results are compared with the slip line results. Since the elastic strains are of order 10^{-3}, the difference cannot be attributed to the elastic terms in the finite element calculations alone. The implication is that the plastic part of the logarithmic strain falls off from about $\ln(b/b_o)$ on the tip more rapidly in the finite element solution, where b_o is the undeformed notch width.

The shape for a blunted initially sharp crack,calculated by RJ,is drawn in figure 2b and it differs from all shapes in figure 2a by only negligible amounts. Since the shapes in the finite element calculations have prevailed for several increments of load, the solution must have reached the stage at which the original notch shape is of no significance to the solution for near tip velocities. Thus the increment of displacement of the point on the blunted notch tip lying on the x-axis may be divided by the increment of notch width to predict the amount,in terms of crack tip opening displacement,

that an initially sharp crack would be pulled forward towards the point two crack widths ahead of the tip. On this basis the shapes from the finite element solutions have been drawn in figure 2b as the shapes for blunted initially sharp cracks, since the negligible difference in shape between the results for blunted shape of a notch and of a sharp crack, as deduced from RJ, indicates that this may be done.

3.2 Stress and plastic strain distributions around blunted notch tips

In figures 3-6 the true stress $\sigma_{\theta\theta}$ (see inset figure 3) is plotted against the distance from the notch tip in the undeformed configuration for each of the four materials for which calculations were carried out. The distance is normalized by the current notch width, which allows results from the later increments of the finite element calculations to be plotted together (McMEEKING, 1976). As the notch tip is approached at a given angle to the crack line in the undeformed configuration, the stress rises in all cases due to increasing triaxial strain. However, the hydrostatic stress cannot be maintained on the blunted notch surface and as a result there is a maximum for $\sigma_{\theta\theta}$, coinciding with a maximum for hydrostatic stress, some distance from the notch tip. As the crack line ($\theta = 0$) is approached on a circular arc of any radius R starting from $\theta = \pi/2$, the stress $\sigma_{\theta\theta}$ rises in each material, and so the $\sigma_{\theta\theta}$ stress at the stress maximum point on $\theta = 0$ is the largest principal stress except for stresses near the blunted tip in the hardening materials.

One effect of power law hardening is to raise the magnitude of the stress at the maximum on each angle to the crack line and to move the positions of the stress maxima closer to the notch tip. Another hardening effect is the upturn in stress close to the notch surface in figure 5, which arises from the elevation of flow stress by the large plastic strains in this area.

The effect, although only apparent in the strongly hardening material of the finite element calculations, would be present in any power law hardening material over a small area,and its absence from figure 4 is just a result of elements on the notch surface relatively large compared to the small area of stress elevation. In fact,when a sharp crack in a power law hardening material is blunted to a finite width, infinitely large stress on the notch surface will arise,but again the large stresses will appear only over a distance small compared to the blunted crack width.

For comparison the stress $\sigma_{\theta\theta}/\sigma_o$ on the crack line ($\theta = 0$) from the RJ slip line solution for the initially sharp crack has been plotted on figures 3 and 5. This is derived from the slip line field shown in the inset, figure 7 and the point at which the stress reaches $3\sigma_o$ coincides with the point S at the outer extent of the spiral slip line region. The stress levels for the power law hardening materials,based on the RJ solution,shown in figures 4 and 5 are approximations in which the plastic strain of the slip line solution is used to calculate the deviatoric stress from the hardening law. The equilibrium equations are integrated, subject to the known deviatoric stress and the traction free boundary condition on the crack surface, to obtain the hydrostatic part of the stress. The agreement between the finite element results and the slip line results and approximations is quite close as far as the position and magnitude of the stress maximum is concerned. This would seem to confirm that the finite element results for the initial notch have developed to the extent that they represent quite well the situation for the blunted initially sharp crack. This suggests that the RJ slip line solution and approximation for the sharp crack underestimates the magnitude of $\sigma_{\theta\theta}/\sigma_o$ at the maximum by 8% for $N = 0.1$, $\sigma_o/E = 1/300$ and by 6% for $N = 0.2$, $\sigma_o/E = 1/300$, and establishes the position of the maximum to within 5%. In view of this the results for stress

$\sigma_{\theta\theta}/\sigma_o$ on $\theta = 0$ derived by RJ for various values of N and σ_o/E are plotted in figure 7. The distance scale in this figure has been developed using the relationship

$$\delta_t = 0.6K^2[\tfrac{2}{\sqrt{3}}(1+\nu)(1+N)\sigma_o/(NE)]^N/(\sigma_o E)$$

as discussed in section 3.4 rather than $\delta_t = 0.61K^2/\sigma_o E$ as used by RJ to develop their figure 10.

Further from the notch tip than the stress maxima, the stresses calculated by finite elements in figures 3-6 agree with the small geometry change finite element calculations of RICE and TRACEY (1973) and TRACEY (1973,1976). The maximum values of mean normal stress in the notch blunting finite element calculations are $2.4\sigma_o$ ($N = 0$), $3.11\sigma_o$ ($N = 0.1$) and $4.13\sigma_o$ ($N = 0.2$) and all lie on $\theta = 0$. When these quantities are divided by the flow stress at the point where they occur, the resulting numbers are close to the predictions of HRR for the maximum value of the ratio of mean normal stress to flow stress on $\theta = 0$ near the crack tip in the respective materials.

The plastic strain plots shown in figures 3-6 are composites of the results from the later increments in the finite element solutions (McMEEKING, 1976). They show clearly that the strains are small except where close to the blunted tip. Outside of the near tip region the larger plastic strains are on the lines at an angle to the crack line, in agreement with known shapes of the plastic zones for plane strain conditions. However, very close to the blunted surface, in the region where the strains are too large to appear in the figures, the plastic strain at a given value of R on the crack line is greater than the plastic strain in positions at angles to the crack line at the same distance from the tip, R. There is little difference between the plastic strain distributions arising in the four

different materials for which finite element calculations were made, and the plastic strain on $\theta = 0$ in each case is similar to the plastic strain on $\theta = 0$ in the RJ slip line solution as plotted in figures 3 and 6. This lack of difference of plastic strains between the different materials, hardening and non-hardening, indicates why RJ's approximations for stress in hardening materials, as plotted in figure 4 and 5, turn out to be so accurate when compared to the finite element results.

3.3 Steady state solution

The results discussed in the previous two sections confirm that steady state solutions as discussed in section 2 have arisen in the later increments of the finite element solutions. Of importance to this conclusion are the facts that the blunted tip shapes change only in size rather than shape in the later increments, and that the stresses and plastic strains from these later increments all fall on one plot, when distance from the tip is normalized by notch width. As a consequence, the shapes in figure 2 and the plots in figures 3-6 may be used as results for blunted sharp cracks with the quantity b in figures 3-6 interpreted as the crack tip opening displacement δ_t.

One difficulty arises in comparing the results for blunted sharp cracks with those for notches. That difficulty is the elevation of flow stress on the blunted surface for power law hardening materials as discussed in section 3.2. This problem is not considered to be severe in view of various aspects of the physical problem being modelled, as follows; (a) the area over which the singularity dominates in the sharp crack case is small, i.e. over an area lying within $\delta_t/4$ of the notch surface in the underformed configuration in the most severe case ($N = 0.2$); (b) power laws as models for hardening have the consequence that infinite plastic strains produce infinite flow stresses, whereas a saturation to constant flow stress after large

plastic strains seems more likely; (c) few cracks are likely to be atomistically sharp and the finite radius at the tip of most real cracks will lead to only large but finite plastic strains at the tip.

3.4 Relationship of crack tip opening displacement to applied load

As discussed in section 3.1, the shapes of the blunted notches in figure 2 allow no unique definition of notch width. An arbitrary choice of definition point for notch width has been made for figure 8, in which the notch width has been measured at the node which lay at the intersection of the straight flank and the semi-circular tip of the undeformed notch. In figure 8, the notch width so defined is plotted versus J_{app}, the value of the J-integral (RICE, 1968) computed on a remote path around the notch tip. The definition of the J-integral is

$$J = \int_{\Gamma} [W dX_2 - \underset{\sim}{T} \cdot \frac{\partial \underset{\sim}{u}}{\partial X_1} dS] \quad , \tag{6}$$

where T is a path in the undeformed configuration from the bottom surface of the notch through material to the upper surface of the notch, $\underset{\sim}{X}$ is the position of a material point in the undeformed configuration, $\underset{\sim}{u}$ is displacement, $\underset{\sim}{T} = \underset{\sim}{n} \cdot \underset{\sim}{t}$ where $\underset{\sim}{n}$ is the outward normal to the integration path and $\underset{\sim}{t}$ is the nominal (1st Piola-Kirchhoff) stress tensor($t_{ij} = \tau_{pj} \partial X_i / \partial x_p$), dS is an element of path length and

$$W = \int_0^{\partial u_i / \partial X_j} t_{ji} \, d(\partial u_i / \partial X_j) \quad .$$

A consequence of the definition of J is that the integral is path independent for elastic materials (linear or non-linear). In addition the relationship

$$J_{app} = (1 - \nu^2) K^2 / E \tag{7}$$

applies to linear elastic materials and to elastic-plastic materials with small scale yielding.

The value of J_{app} used in figure 8 was inferred from the finite element results of RICE and TRACEY (1973) and TRACEY (1973, 1976) by assuming that J is essentially path independent outside their elements immediately adjacent to the tip (an assumption shown to be correct by PARKS (1975)). The plots in figure 8 clearly show that a linear relationship arises between notch width and J_{app} quite early in the loading history. This linearity presumably associates with the occurence of the steady state solution, and may be used to relate crack tip opening displacement to applied load for an initially sharp crack. This follows from noting that the width of the blunted notch can be interpreted as the width of a blunted crack plus the original notch width. In particular the increment of notch width for an increment of load can be used as the increment of crack width during the same increment of load. Thus the terminal slopes in figure 8 can be used for the slopes of the crack tip opening displacement, δ_t, versus J_{app}/σ_o straight lines, which pass through the origin. These slopes are the values n in column I of the table, which contains in the additional columns values for n obtained from plots of notch width J_{app}/σ_o when other positions are chosen for defining notch width. Note that the crack tip opening displacement, measured at the elastic-plastic boundary for both non-hardening materials, is about the same for given J_{app} despite the differences nearer the tip. Indeed it is arguable that all four cases have basically the same crack tip opening at the elastic-plastic boundary under the same load J_{app}, in striking similarity to the findings of RICE (1967b) in the anti-plane shear case. The values for n in column I of the table for the material with $\sigma_o/E = 1/300$ fit quite closely to the relationship, suggested by RICE (1973),

$$\delta_t = 0.55 J_{app}/\bar{\sigma}_{flow} \quad , \tag{8}$$

where $\bar{\sigma}_{flow}$ is the flow stress in tension at an equivalent shear strain of $N/(1 + N)$, or

$$\delta_t = 0.55 J_{app}[\tfrac{2}{\sqrt{3}}(1 + \nu)(1 + N)\sigma_o/NE]^N/\sigma_o \tag{9}$$

In addition, the values n for the same material in column II fit (8) and (9) with 0.55 replaced by 0.58. This agrees with calculations by TRACEY (1973), who found that the relationship $\delta_t = 0.54 J_{app}/\bar{\sigma}_{flow}$ arose for small scale yielding in his finite element solutions for hardening and non-hardening materials using crack tip singularity elements and a definition of crack tip opening displacement like that used for column II of the table. PARKS (1975) has recently suggested that the number in TRACEY'S relationship should be 0.65 in view of the undesirable path dependence of J within TRACEY'S non-hardening singularity element, which reduces the value of J at the crack tip to 0.8 of the remote value of J. More recently TRACEY (1976) has suggested $\delta_t = 0.54(1 + N)J_{app}/\bar{\sigma}_{flow}$ based on results using the non-hardening singularity element, which has path dependent J within it, and a hardening singularity element with path independence of J.

Other determinations of n have been made for non-hardening materials based on estimates for velocities on slip lines near the crack tip. RICE (1968) suggested $\delta_t = 0.67 J_{app}/\sigma_o$ and RJ used the non-hardening limit of the HRR singularity to obtain $\delta_t = 0.79 J_{app}/\sigma_o$.

An experimental attempt to measure n has been carried out by ROBINSON and TETELMAN (1974) using standard ASTM K_{IC} specimens of AISI 4340 steel. Cracks in loaded specimens were infiltrated by a fast setting plastic and the measurements of crack tip opening displacement were made on the carefully withdrawn casts. Their results gave $\delta_t = J_{app}/\sigma_o$, a somewhat larger δ_t than would be predicted from all the analyses discussed previously. Indirect

measurements of δ_t may be made if one assumes that the stretched zone between the pre-fatigued crack surface and the fast fracture area on the fracture surface of broken specimens is the perfect remnant of the severely strained blunted tip surface, and that as a consequence the stretched zone size would be controlled by the value of K at fracture. BROTHERS et al. (1971) measured stretched zone widths in broken specimens meeting ASTM specifications for K_{IC} testing in steel, aluminum and a titanium alloy, and, based on a shape for the blunted tip as in figure 2, their measurements suggest a value for n in the region of 0.7. for all these materials. GREEN, SMITH and KNOTT (1973) noted that the measurements by BATES and CLARK (1969) of stretched zone width on fracture surfaces on broken fracture toughness specimens, made from various structural steels, could be correlated with $\delta_t = 0.63\ J_{app}/\sigma_o$. BROEK (1974) however has found that stretched zone width in some aluminum fracture toughness specimens does not correlate with K_{IC}, but that twice the difference in height across the stretched zone is $0.4\ K_{IC}^2/\sigma_o E$, suggesting the value 0.44 for n.

3.5 Path dependence of the J-integral in the finite element results

Path integral calculations of J, as defined in (6), were made on various contours around the notch tip. The contours were straight lines within an element passing through the centroid of the element, and centroidal values of the integrand were used as the integrand over all of the path within the element. The distance from the centre of the notch tip to the centroids of all the elements on a given path was about the same, and this distance is represented by the distance R in fig. 9. The contours on which the calculations were made are: (i) through the inner layer of elements of section B of fig. 1 excluding all but one element on the straight flank; (ii) through the outer layer of elements of section B; (iii) through the second outermost ring of elements of section A;

(iv) and through the outer ring of elements of section A. The displacement gradients, $\partial u_i/\partial X_j$, necessary to compute the term $\underset{\sim}{T}.\partial u/\partial X_1$, were obtained by numerically integrating the expression $\partial v_i/\partial X_j = (\partial v_i/\partial x_k)(\partial x_k/\partial X_j)$ using the quantities $(\partial v_i/\partial x_j)\Delta t$ calculated at each step of the finite element calculations. Here Δt is the time step size of the finite element increment, in which time is to be understood as a parameter of the applied load and is zero in the undeformed configuration. Similarly the term W was calculated from the relationship $W = \int_0^{t_f} \tau_{ij} D_{ij} dt$, where t_f parameterizes the load causing the deformation state for which W is to be calculated, and the reference state for $\underset{\sim}{\tau}$ is always the undeformed state.

The values for J, so computed, are plotted in fig.9 normalized by the value J_{app} calculated on a remote contour. The values of J/J_{app} for values of R/b greater than twelve are all close to unity, indicating that path independence of J prevails over all but a small area of the mesh. The area where J is path-dependent, i.e. R/b less than about 6, is also the area significantly affected by the blunting of the notch. The results shown in fig. 9 were calculated on three contours, but seem to fall on one curve indicating that $J \to 0$ as $R \to b_o$. The points showing $J/J_{app} = 1$ for R/b less than 12 actually arise in the elastic solution to the problem and in the first few plastic increments, during which J has to be path independent for contours separated by elastically deforming material. The reason for the extreme path dependence of J as computed for $R/b<1$ is not clear. The calculations were checked to ensure that no intense deformation contributing to the notch opening was occurring outside of the contour, and thus failing to contribute to the computed values of J. No significant improvement of the results towards path independence of J was obtained in this way. It is instructive, however, to consider the contour Γ_t on

the undeformed notch tip surface, in which case

$$J_t = \int_{\Gamma_t} W dX_2.$$

If it is assumed that a good approximation is $W = \sigma_o \bar{\varepsilon}^p$ on Γ_t for large amounts of opening, an assumption which seems to be borne out by the actual calculations of W in the near tip region, and that the near tip plastic strains after large amounts of opening are proportional to $\ell n(b/b_o)$, which is also confirmed by the finite element results, then J_t/J_{app} will diminish as b/b_o increases, since J_{app} is basically proportional to $(b/b_o - 1)$ after large opening as can be seen in fig. 8. The question here is whether the plastic strains on Γ_t as inferred from the finite element results at discrete points off Γ_t are accurate, but confirmation that they are reasonably accurate is available from the RJ slip line results.

All this argues that fig. 9 is an accurate representation of the path dependence of J, but the possibility still exists that numerical inaccuracy in either the computation of J or the finite element results is the real cause of the path dependence. However, to have achieved such inaccuracy as to have calculated J/J_{app} wrong by an order of magnitude does not seem possible while achieving such good agreement with the results of RJ slip line solution, especially since all the quantities involved in calculating J as a path integral are quite smoothly varying and seem to present no difficulty in the numerical integration. In addition, the calculation of W for material in the near tip region is not sensitive to a choice of loading path slightly different from the actual loading path, so that it does not seem possible that inaccurate finite element calculations of the loading history could have seriously affected the calculation of J in this respect. This also suggests that a deformation plastic material with similar loading characteristics to the Prandtl-Reuss incremental

plasticity material would exhibit a quite different near tip behavior. This may be of some importance in view of the fact that models for polycrystalline slip suggest that vertices may arise on yield surfaces. It has been suggested that constitutive modeling for such a plasticity mechanism is best done using deformation plasticity laws when the loading path is only slightly non-radial (e.g., HUTCHINSON, 1970).

The path independence of J, outside of the region affected by the blunting, agrees with the finite element solutions of several investigators for cracked elastic-plastic bodies obtained using the conventional small strain assumptions, ignoring the effects of blunting. Path dependence of J quite close to the crack tip under contained yielding conditions has been noted by KOBAYASHI, CHIU and BEEUWKE (1973) and HAYES and TURNER (1974) and by PARKS (1975) in the work of TRACEY (1973) and RICE and TRACEY (1973). In the last case a path dependence of J was found in the crack tip singular elements, which persisted when a deformation plasticity constitutive law was used, leading to the conclusion that the path dependence in the singular element may be erroneous. These investigaticns suggest that if J is really as path dependent as indicated by fig. 9, then the path dependence can be observed only when a geometrically non-linear approach to the contained yielding crack tip plasticity problem is utilized. In the non-linear solution, (ie; notch blunting by finite elements), J is found to be path independent in the part of the problem where geometrically non-linear effects are small, and to be path dependent where non-linearity dominates, ie; close to the blunted tip.

A method of solving crack tip plasticity problems for the near tip fields involves an assumption that J is path independent right into the crack tip, as in the work of RICE (1968) and HRR. Since it has been shown that the inclusion of the geometrically non-linear terms in the problem seems to lead to a path

dependence of J near the crack tip, the question arises of whether the results based on path dependence of J are correct. It appears that the answer to this is based on the different role the crack tip plays in the linearized and non-linear formulations. In the geometrically linearized case, (RICE, 1968 and HRR), the crack tip is modeled as a singular point for strain, with the strength of the singularity determined by the hardening characteristics and the amplitude controlled by J. The resulting field of singular strains around the crack tip involves mostly shearing adjacent to the tip, and it is these shear strains that give rise to the opening displacement at the crack tip. The non-linear formulation of RJ illustrates most simply the difference from the singularity approach. In this the velocities around the crack, developed from the path independent J singularity analysis of RICE (1968), are used to set boundary conditions on a zone of spiral slip lines in which intense stretching occurs (see inset fig. 7). These velocities would cause a shear strain singularity if they were applied to one point, as they are in RICE (1968), but now they are applied along the boundary line of the spiral zone, and the shearing is intense but non-singular. This shearing is still accomodated by the crack opening, but account is now taken of the necessary stretching ahead of the crack tip. Thus, it may be seen that the spiral zone and blunted tip has replaced the crack tip point and singular behavior of the RICE (1968) and HRR work, with the outer field of that work substantially unaltered by the geometric effects of blunting. Since the notch blunting finite element calculations produce results almost identical to the RJ work, the explanation of the apparent limited path dependence of J in the finite element results for blunting seems to be associated with this idea of a dominant outer field, in which J is path dependent, surrounding the perturbed blunted area. The conclusion is

then that the small strain singularity work, based on path independence of J, correctly predicts the outer field and that the outer field is only perturbed locally by the blunting.

4 NON-SMOOTH BLUNTING OF CRACK TIPS

The results of section 3 apply to crack tips which have experienced only smooth blunting as opposed to blunting to shapes with sharp corners. If sharp corners do occur in the steady state crack tip blunted shape, the crack tip opening has been accomodated at least partly by singular shear strain rates (but bounded strains, of order unity) at the vertices on the crack tip. This has the effect of transporting material from the interior onto the crack tip surface. In the slip line fields around blunted crack tips with vertices, shown in fig. 10, it can be seen that a fan of slip lines associated with the singular shearing emanates from each corner on the crack tips. There are similarities to the RJ slip line field in that the zones, bounded by the crack tip and the slip lines AB and AC, are partly filled up by spiral slip lines in which large amounts of stretching take place. Intense stretching may take place within the other areas of slip lines in the zone bounded by AB, AC and the crack tip, but some, if not most, of the crack opening is accomodated by the localized shearing in the fans, so the stretching of material will not reach the levels attained in the smoothly blunted case. The overall similarity of the slip line configurations in fig. 10 to the slip line field for the smoothly blunted crack is striking and the possibility of either smooth or vertex blunting occurring with similar velocity fields remote from the crack tip is apparent. The limited levels of plastic strains, when sharp crack tips are blunted into tips with sharp corners, seems to suggest that these shapes are more stable than smoothly blunted tips when hardening constitutive laws are used. However, the tendency for deformation to localize at, say, asperities on the tip surface (McCLINTOCK, 1971, pp 158-160) may be important in this respect.

The slip line fields in fig. 10 are those presented by McCLINTOCK (1971, pp. 158-159) for steady state blunted crack tip shapes, and the included angle of the tip in the case where there are three corners on the tip is 120°. The stress state in both cases is such that further from the tip than A, $\sigma_{yy} = 2.96\sigma_o$ on $y = 0$. In the flat nosed case, the stress $\sigma_{yy} = 1.16\sigma_o$ between E and D, and rises monotonically from this value at D to $2.96\sigma_o$ at A. In the sharp nosed case $\sigma_{yy} = 1.79\sigma_o$ between G and F, and rises monotonically from this value at F to $2.96\sigma_o$ at A. Thus the flat nosed case is similar to the non-hardening smooth blunting case, in that σ_{yy} on $y = 0$ at the smooth tip surface is $1.16\sigma_o$ and rises to $2.96\sigma_o$ some distance from the tip surface. When non-hardening materials are compared, the sharp nosed case provides a severe state of high stress and large plastic strain at the crack tip surface, not present in either the flat nosed or smoothly blunted case. This severe state, however, prevails only over a small area adjacent to the crack tip.

Of course, the cases shown in fig. 10 are only two members of an infinite family of vertex shapes into which blunting can occur. An example of a blunted notch with at least five vertices on the tip is presented by CLAYTON and KNOTT (1976), in which the vertices seem to be forming by the asperity localization mechanism suggested by McCLINTOCK (1971, pp 158-160).

5 VOID GROWTH NEAR THE CRACK TIP AND FRACTURE INITIATION

Determination of the shapes and sizes of voids growing near the crack tip is a step in constructing a ductile fracture model based on the coalescence of these voids with the crack tip. One aspect of the problem pertains to void nucleation, typically from the cracking of second phase inclusions or precipitates, and appropriate calculations of void growth must be based on initial conditions prevailing at void nucleation. Although void nucleation is the subject of a great deal of research (e.g. GURLAND and PLATEAU (1963), ASHBY (1966), TANAKA, MORI and NAKAMURA (1971) and ARGON and IM (1975)), the results are not yet so conclusive that conditions of nucleation can be used in the void growth calculations. However, by using an initial condition that the void nucleates from the particle with a spherical shape when the particle first enters the plastic zone, the result will be an underestimation of toughness given that all other aspects of the model are accurate. The formulation of RICE and TRACEY (1969) for the rate of growth of a spherical cavity in a remote uniform stress and plastic strain field may be used to compute the size of the voids growing in the near tip field as computed by finite elements. This approach has already been taken by RJ, but for voids in the near tip field as computed by the slip line method in their blunting analysis. The results of RICE and TRACEY, which are similar to those of McCLINTOCK (1968a) for a long cylindrical cavity, show a strong dependence of the growth on mean normal stress. The velocities on the surface of the spherical void are approximately compatible with the homogeneous deformation rate $\underset{\sim}{D}^V$ of the void interior given by

$$\underset{\sim}{D}^V = 2\,\underset{\sim}{D}^\infty + 0.279\,\dot{\bar{\varepsilon}}^p\,\underset{\sim}{I}\,\exp(3\sigma^\infty/2\sigma_o)\ , \qquad (10)$$

where $\underset{\sim}{D}^{\infty}$ is the remote uniform deformation rate (deviatoric) in the rigid plastic material, $\dot{\bar{\varepsilon}}^{p}$ is the equivalent plastic strain rate ($\dot{\bar{\varepsilon}}^{p} = (2D^{\infty}_{ij}.D^{\infty}_{ij}/3)^{1/2}$), $\sigma^{\infty}/\sigma_{o}$ is the ratio of mean normal stress to yield stress in tension in the remote field, and $\underset{\sim}{I}$ is the identity tensor. To modify (10) so that void growth rates in the non-homogeneous stress and strain fields around the crack tip may be approximated, the stresses and strain rates at the current void site, computed as if the void was not present, may be substituted for all quantities in (10) identified with the remote field. This ignores perturbation of the local stress and strain fields at the void site by the presence of the void. As the void grows it becomes non-spherical, so an approximation is introduced based on a substitute spherical void with diameter $\bar{a}$ chosen so that the substitute void has the same volume as the actual void. Since this sphere would be subject to the deformation rate $\underset{\sim}{D}^{V}$ as given by (10), the velocity at point S on the surface of this void in the absence of spin is

$$\underset{\sim}{v}^{p} = \bar{a}\underset{\sim}{D}^{V}.\underset{\sim}{n}^{s} \quad , \tag{11}$$

where $\underset{\sim}{n}^{s}$ is the unit vector from the centre of the sphere towards the point S. The spherical void may be deformed into the actual void by the deformation $\underset{\sim}{V}^{V}a_{o}/\bar{a}$, where a_{o} is the diameter of the original undeformed spherical void and the deformation gradient $\underset{\sim}{F}^{V}$ ($F_{ij} = \partial x_{i}/\partial X_{j}$) within the homogeneously deformed ellipsoidal void can be decomposed as in $\underset{\sim}{F}^{V} = \underset{\sim}{V}^{V}.\underset{\sim}{R}^{V}$, where $\underset{\sim}{R}^{V}$ is the rotation experienced by the actual ellipsoid. In particular the vector $\bar{a}\underset{\sim}{n}^{s}$ is deformed into $a_{o}\underset{\sim}{V}^{V}.\underset{\sim}{n}^{s}$, and this last vector may be used to define $\underset{\sim}{n}^{p}a_{act} = a_{o}\underset{\sim}{V}^{V}.\underset{\sim}{n}^{s}$, where $\underset{\sim}{n}^{p}$ is a unit vector and $\underset{\sim}{n}^{p}a_{act}$ is the position vector of point S on the ellipsoidal void surface. The approximate deformation rate

in the ellipsoidal void is chosen so that v^p is the velocity of the point at $\underset{\sim}{n}^p a_{act}$ on the ellipsoidal void surface, and so

$$\underset{\sim}{v}^p = (\dot{\bar{a}}/a_o)\underset{\sim}{D}^v.(\underset{\sim}{V}^v)^{-1}.\underset{\sim}{n}^p a_{act} \quad . \qquad (12)$$

The spin tensor $\underset{\sim}{\Omega}(2\Omega_{ij} = \partial v_j/\partial x_i - \partial v_i/\partial x_j)$, at the void site causes an additional velocity of $-\underset{\sim}{\Omega}\cdot\underset{\sim}{n}^p a_{act}$ at that point, and from this it is simple to show that

$$\dot{\underset{\sim}{F}}^v = (\underset{\sim}{D}^v.(\underset{\sim}{V}^v)^{-1}\dot{\bar{a}}/a_o - \underset{\sim}{\Omega}).\underset{\sim}{F}^v \quad . \qquad (13)$$

This equation was numerically integrated using the steady state results from the finite element analysis of blunting, with the computation started when the void site enters the plastic zone. The plastic part of the local deformation rate was used as $\underset{\sim}{D}^\infty$ in (10). The results for the non-hardening material with $\sigma_o/E = 1/300$ are shown in fig. 11 and show that the void at 45° experiences faster earlier growth due to the larger amounts of plastic strain occurring there. The void at 0° catches up and grows faster when it is close to the crack tip due to larger mean normal stresses. The results for the void at 0° confirm the similar calculations of RJ based on their slip line results for blunting. The growth rates in the hardening material with $N = 0.1, \sigma_o/E = 1/300$, as in figure 12, are not much different from those in the non-hardening material when phrased in terms of crack tip opening displacement, as in fig. 11 & 12. However, when measured against J_{app}, the growth rates in the hardening material are lower than the rates in the non-hardening material.

5.1 Fracture models based on the void growth model

In spite of the approximations involved in obtaining the results in

figs. 11 & 12, the calculations of void size and shape may be valuable in studying the near tip growth in materials with loosely bonded equiaxed second phase particles, which come loose from the matrix as soon as the matrix experiences plastic strain. The particles should be spaced widely enough apart so that void growth is not heavily influenced by neighboring voids. When the void is large enough, it will coalesce with the crack tip, and, if the manner of coalescence is known, the crack tip opening displacement just after the coalescence event may be calculated. Using the arbitrary criterion that coalescence will occur when twice the ligament between the void and the crack is the same size as the maximum dimension of the coalescing void, RJ computed the crack tip opening displacement for fracture in terms of the ratio of void nucleating particle spacing to void nucleating particle size, by assuming that voids on the crack line would coalesce with the crack earlier than other voids. They compared their results (see fig. 13) with data collected by PELLISSIER (1968) and BIRKLE et al (1966) for a high strength steel containing MnS particles and known to fracture in a ductile manner as evidenced by dimpled fracture surfaces. The MnS particles are known to come loose quite readily, although COX and LOW (1974) have recently shown that macroscopic strains larger than 0.1 are necessary to cause 75% or more of the MnS particles to nucleate voids in AISI 4340 commercial purity steel. It might then be expected that the RJ model should agree quite well with the data, but should underestimate the toughness. Although the trend of the data, including those for GREEN and KNOTT'S (1976) C/Mn steel, is captured by the RJ model, an overestimation of the toughness is involved. It is not clear whether this is a result of inaccurate statistical estimation of the model parameters from metallographic studies, since much better agreement may be obtained by using

the three-dimensional nearest neighbor spacing as D, rather than the two-dimensional nearest neighbor spacing which is used as D for all data points except possibly those of GREEN and KNOTT. On the other hand, the overestimation may be associated with inaccurate modeling of the crack-void coalescence event. In the steels with MnS inclusions, the coalescence seems to be controlled by the smaller carbide inclusions in view of a second family of small dimples on the fracture surface shown to be associated with the carbides by COX and LOW (1974) in AISI 4340 steel. As evidenced by the larger fraction of the fracture surface covered by small dimples in the AISI 4340 steel compared with the fracture surface of the steel studied by PELLISSIER, this coalescence seems to occur earlier in the AISI 4340 steel, and may be proposed as the reason for the poorer fracture toughness in terms of critical δ_t/D of the AISI 4340 steel, as shown in fig. 13.

Judging by the micrographs obtained by COX and LOW, the coalescence in 4340 steel occurs by localization of plastic flow in bands containing small voids. These small voids seem to be responsible for the family of small dimples on the fracture surface. The tendency of flow to localize seems to be present to a greater or lesser extent in most of the materials involved in fig. 13. It would seem to be of significance that the 4340 steels perform most poorly as judged by the relative position of the data in fig. 13, since these steels are observed to flow-localize quite readily compared to the other materials. In comparison, COX and LOW observe that the 18-Ni maraging steel both has a higher toughness than 4340 steel and shows little tendency to localization of flow. The localization effect may not be absent entirely from the maraging steels, since PSIODA and LOW (1974) have observed that, when an 18-Ni maraging steel is heat treated to different strength levels, a correlation of the fraction of

the fracture surface covered by smaller dimples may be made with yield strength and fracture toughness. As the yield strength increases, the fracture toughness drops and an increasing fraction of the fracture surface is covered by the family of smaller dimples. Concurrently, an increasing tendency for voids in sectioned specimens of all these steels to be linked by sheets of smaller voids has been observed, and it is believed that this is evidence of localization of plastic flow either caused by or causing the nucleation of voids from smaller particles. A similar explanation seems to be suitable regarding the difference between the data for 2000 series and 7000 series aluminum alloys deduced by RICE from the work of VAN STONE et al (1974) and shown in fig. 13. Both types of alloy have inclusions which nucleate voids after a few percent strain, and it appears that not all inclusions actually provide voids even at high strains. Thus the RJ model would seem to be an underestimation of the toughness for both alloys. This is not so and once more an extensive family of small dimples is apparent on the fracture surface, suggesting coalescence of crack and void much earlier than supposed by RJ. The 7000 series alloys show larger fractions of fracture surface covered by small dimples, and, if the explanation of localization of flow is accepted, this seems to suggest that localization occurs more readily in the 7000 series than in the 2000 series. VAN STONE and PSIODA (1975) have observed the formation of a void sheet in 2124-T851 alloy, and the family of small dimples probably arises from such localized deformation. In seeming confirmation of this, HAHN and ROSENFIELD (1975) have noted that as the yield strength of 7178 aluminum is increased by aging, the fracture toughness falls and then, during overaging, the fracture toughness rises while the yield strength falls, and they observe that in peak aged condition another 7000 series alloy shows a tendency for plane strain

flow to localize into bands containing small ruptured particles.

The similarity of GREEN and KNOTT'S (1976) data shown in fig. 13 for the initiation of crack growth in fully plastic three point bend specimens and the data for steel under small scale yielding conditions suggests that the crack tip processes are similar in both cases. GREEN and KNOTT noted that in a free cutting mild steel which strain hardened appreciably, (open circles, fig. 13), the crack growth initiation occurred by the growth and coalescence of voids, and the model of RJ predicted the critical point for crack growth initiation quite well. However, in a prestrained specimen which basically was non-hardening, the crack growth initiation occurred by localized shearing, and, as can be seen in fig. 13, the initiation of crack growth occurs much earlier in this specimen than in the non-prestrained specimen. CLAYTON and KNOTT (1976) have also observed that increasing prestrain in HY80 steel leads to smaller crack tip opening displacement at crack growth initiation and also increasing localized flow at the crack tip.

All the data discussed so far are for materials with inclusion not well bonded to the matrix. By changing the orientation of the specimens of ENIA so that the inclusions were elongated in the direction normal to the crack line (longitudinal specimen, fig. 13), GREEN and KNOTT found that crack growth initiation required much larger crack tip opening displacements. They argued that this orientation is much less favourable for the nucleation of voids at the particles and so that much less void growth occurs in the near tip field. Similarly, the data for the ductile fracture of mild steel with relatively tenacious spheroidized carbide particles taken from the work of RAWAL and GURLAND (1976) does not follow the RJ model very well. However, it should be noted that for these materials the trend of increasing δ_t/D correlates

with diminishing size of the carbide particles. Since GURLAND and PLATEAU (1963) and other have noted that larger particles crack earlier than smaller particles, the increasing toughness relative to the prediction of RJ seems to be readily explainable.

In conclusion, it seems to be the case that the fracture toughness of materials with inclusions not well bonded to the matrix can be predicted quite well by the model of RJ. The differences between the model and the data and between materials seems to be the most easily explained in terms of the relative tendency for deformation to localize in bands associated with the nucleation of voids from smaller particles, which ultimately form the family of small dimples on the fracture surface. If the larger inclusions do not readily nucleate voids, the RJ model is not appropriate but it may be modified to account for void nucleation.

The same criterion as used by RJ may be combined with the results plotted in fig. 11 for $\theta = \pi/4$ and all results in fig. 12 to produce a criterion for the initiation of crack growth. While the predicted toughness from these in terms of crack tip opening displacement will be different from those predicted by RJ, the difference from the results of RJ will be slight compared to the difference between the data and the predicted toughness in fig. 13. Of course when the predicted toughnesses are phrased in terms of K or J_{app}, hardening materials will have a predicted toughness greater than the toughness of the non-hardening materials when all other properties are the same. This is in agreement with the known trend of greater plane strain fracture toughness with lower yield strength and greater hardening as noted by KRAFFT (1964).

5.2 Crack-void coalescence and void nucleation

Although many aspects of the fracture model just described are highly

approximate, the two aspects which seem most in need of improved modeling are the coalescence event and the nucleation of the void. Improved understanding of the coalescence event might allow calculations of toughness somewhat lower than predicted from the model by RJ, while void nucleation requiring other than negligible stresses or plastic strains will lead to higher predicted toughness as already discussed. Some possible models for the coalescence event include localization of flow in the ligament, nucleation of voids from families of smaller particles in the ligament and the thinning down of the ligament completely. In non-homogeneous deformation it is known that rigid-plastic materials can be subject to localized shearing along the slip-lines (HILL, 1950, pp. 149-150). Thus it may be that localization may occur in non-homogeneously deformed elastic-plastic materials along contours which are everywhere tangential to the principal shear directions after the hardening rate everywhere on the contour falls to a sufficiently low level. The dominant role of hardening and strength level in localization of flow, as noted in section 5.1, suggests that a proper study of stresses and strains in the ligament between the void and the crack should be based on more realistic hardening laws than a pure power law. Possibly it should include the effects of porosity, from widely nucleated voids, in reducing the hardening rate of a macroscopic element of a material as noted in the localization study of BERG (1970). The coalescence of void and crack after localization of flow has occurred is proposed to arise from heavy nucleation of voids from small particles in the band of localization. The presence of voids nucleated from particles in bands of localized deformation has been reported by ROGERS (1960) in copper and by BLUHM and MORRISEY (1968) in copper and steel in addition to the observations of LOW and co-workers discussed in section 5.1. However, this evidence is equally suggestive of a coalescence

event caused by nucleation of a few voids from smaller particles in the ligament starting a spreading band of nucleating voids, continuing until the ligament is broken. The other possibility for coalescence, the thinning down of the ligament to zero thickness, may only be possible in the absence of smaller particles which can nucleate voids, and in addition the material might have to have sufficient hardening capacity to avoid a possible localization of flow.

The improvement of the modeling of void nucleation may be of importance for understanding both the coalescence event and the formation of the voids from the larger particles. ARGON and IM (1975) have studied a moderately hardening spheroidized 1045 steel and they concluded that the closely spaced Fe_3C particles separate from the matrix when a tensile stress, which happens to be equal to 3.5 times the tensile yield stress of the material, acts in the neighborhood around the particle. Assuming that this critical stress has an absolute meaning, its high level indicates that, for example, the void could not nucleate in a non-hardening material in the crack tip region, and that it could nucleate on $\Theta = 0$ in the $\sigma_o/E = 1/300$, $N = 0.1$ material used in the finite element calculations but not on the line $\Theta = \pi/4$ in the same material. This discrimination would indicate that, although all the growing voids will be smaller than indicated by figs. 11 & 12, the voids off the crack line will be reduced in size more than those on the crack line.

GURLAND (1963) has suggested that a critical plastic strain, (equivalent to a critical shear stress), is necessary to nucleate voids from particles, and a consequence of this would be the nucleation of voids off the crack line, further from the crack tip, than on the crack line, except from the most tenacious of particles. Again all the growing voids will be reduced in size

compared to figs. 11 & 12 but now the voids on the crack line will be reduced more than the voids off the crack line. McCLINTOCK (1968b) has suggested a combined critical stress and strain criterion in which a high strain and a low stress or a low strain and a high stress could both nucleate voids. Confirmation of this seems to be evident from the work of MACKENZIE, HANCOCK and BROWN (1973) on several steels, in that the formation of a large void from smaller voids nucleated from particles consistently followed this sort of criterion, in terms of mean normal stress and plastic strain. Their data indicates, for example, the nucleation of these voids more favourably off the crack line in HY130 steel.

5.3 Other fracture models and criteria

KRAFFT (1964) has proposed a model for ductile fracture by coalescence of a crack and void in which, basically, the coalescence will occur when the tensile instability strain is achieved at the crack tip over a size scale equal to the spacing of void nucleating particles. As suggested by CLAUSING (1970), the plane strain ductility may be more useful for quantifying this necking model, and some successful correlation (e.g. OSBORNE and EMBURY, 1973) has been carried out using this and the tensile instability strain, despite the indirect link between macroscopic ductility and microscopic processes. Another model for fracture, which might be useful for materials where the spacing of the particles first nucleating voids is about the same as the sizes of the particles themselves, is that, as soon as the voids are nucleated, initiation of crack growth occurs. The criterion for fracture arising from this would involve the conditions for void nucleation extending over one or two particle spacings. As has been discussed in section 5.2, it is not certain whether stress, plastic strain, or a combination of stress and strain would comprise

the void nucleation criterion. In the case of slip nucleated cleavage in mild steel, RITCHIE et al (1973) have successfully applied a stress criterion based on a critical cleavage stress and they found that fracture occurred when the critical stress was achieved near the crack tip over a size which happened to be equal to two grain sizes. RAWAL and GURLAND (1976) have also noted that a critical stress was achieved over a distance of about 1.3 grain sizes in their specimens of spheroidized mild steel, which failed by cleavage. In each of these models the fracture criterion involved critical conditions achieved over some distance. Indeed McCLINTOCK (1958), RJ and RITCHIE et al (1973) have all pointed out that such criteria require the inclusion of a critical distance, to avoid the prediction of fracture for vanishingly small loads. Some brief comments may be made on each type of fracture criterion in the light of the finite element results as illustrated in figs. 3-6.

(a) Stress criteria: Since the tensile stress and the hydrostatic stress are greater on the crack line than off the line, this type of criterion will always be based on models involving crack growth straight ahead on the crack line. In addition, the stress levels (except for the flow stress very near the tip) are limited and are proportional to the tensile yield strength. This can be used to predict a transition, associated with decreasing strength level, from the fracture mode controlled by stress to some other fracture mode as noted by RJ and partly confirmed in the case of the cleavage-ductile transition in steel by RITCHIE et al (1973) and PARKS (1976). A difficulty arises from this, as far as fracture models based on a stress criterion for void nucleation are concerned. If the critical stress to nucleate voids is constant, then the strength level may be reduced until no voids can be nucleated in the near tip field. Since the crack growth can no longer involve this family of voids, a transition to another fracture mechanism must occur.

Such transitions in the ductile fracture range of toughnesses do not seem to occur. However, the objection to stress criteria for void nucleation would not be valid if the elevated flow stresses on the crack surfaces really exist in hardening materials. These elevated stresses could cause the void nucleation at very low strength levels and would involve a prediction of relatively high toughness.

(b) Strain criteria: If the critical strain in the criterion is low, so that the curves for plastic strain in fig. 3-6 may be used, then the critical condition will first be reached over a line at some angle to the crack line and crack growth will occur along this line. In contrast, if the fracture strain is so high that figs. 3-6 cannot be used, the critical conditions will first arise on the crack line and straight ahead crack growth may be predicted. Since the strain levels are not limited except by the crack tip opening displacement, no transition from this fracture mode will occur with decreasing strength level.

(c) Mixed stress and strain criteria: If the fracture model involves an event in which the plastic strain sets the level of critical stress, then a mixed criterion arises. Both (a) and (b) are limiting examples of mixed criteria, and so mixed criteria may involve predictions of transition of fracture mode, flat crack growth, or angled crack growth.

The localization of flow of the kind discussed in section 5.2 may be an important element in some fracture models, over and above its possible role in breaking ligaments between cracks and voids. After some amount of deformation has occurred near the crack, conditions might be such that a localization of flow into a narrow band is favoured over a continuing deformation in the regular near tip mode. The theoretical framework for this has been studied by

HILL (1962), and RICE (1976) has discussed the manner in which localization can occur under very constrained boundary conditions. The localization can set in when the hardening rate has fallen to a low, but possibly non-zero rate. In addition, a lack of normality in the flow rule or the presence of a vertex on the yield surface is favourable to the early inception of localization, as compared to cases with "normality" flow rules or smooth yield surfaces respectively. As before, the fracture would occur by massive nucleation of voids in the band of localization, or by fast growth and coalescence of voids already lying within the band. This model for localization has been discussed by BERG (1970) for porous materials, and as he notes it may be used to predict extensive zig-zag growth of the crack. In the absence of general porosity, VAN DEN AVYLE (1975) has observed such zig-zag growth in fracture toughness specimens of 4340 steel and maraging 300 steel, in which the wavelength of the zig-zag growth could be correlated with K_{IC}. There are no large dimples on the fracture surface and no voids in material near the fracture surface. It may be that the explanation for such crack growth behavior lies in a localization model. The role of hardening in the localization model is illustrated by work of HUFF, JOYCE and McCLINTOCK (1969), who observed fracture along a curved slip line in a fully plastic specimen of hardened 1020 steel, while an annealed specimen fractured along the crack line.

In all the fracture models discussed, a clear indication of the direction of initial crack growth can be made once the details of the model have been worked out. Reversing this point of view, observation of the direction of initial crack growth in small scale yielding might allow one to draw conclusions about the nature of the fracture processes and, along with observation of the void growth around blunted crack tips, this would allow one to assess

the value of particular fracture models. It seems that few investigators have recorded the details of initial crack growth in small scale yielding. However, RAWAL and GURLAND (1976) show a micrograph of a pre-fatigued crack in spheroidized carbon steel which has experienced crack growth by ductile rupture along the crack line, while BEACHEM and YODER (1973) observed angled ductile crack growth from a pre-fatigued crack in 200-grade maraging steel.

6 CONCLUSIONS

It is concluded from the constant crack tip shape and the constancy of the stress and plastic strain distributions, when length measurements are normalized by current notch width, that a steady state solution independent of the original notch shape was achieved in the later increments of the finite element calculations. Thus the solutions obtained can be applied to the problem of the smooth blunting of a sharp crack in an elastic-plastic material under small scale yielding, plane strain, opening loading conditions.

While the results show that tensile stresses are elevated by triaxial strains near the tip of the blunted crack, it is seen that the stress levels arising from this effect are limited and a maximum for stress lies a distance of about 2 crack tip openings from the notch tip, measured in the undeformed configuration. The distance between the stress maximum and the crack tip depends on the amount of hardening; it decreases in terms of crack tip opening as the power law hardening exponent increases. At distances closer to the tip than that of the stress maximum, the tensile stress falls off due to diminishing constraint. It is only in this area that equivalent tensile plastic strains are large and, in fact, they are larger than about 0.1 only within a distance of one crack tip opening from the crack tip, as measured in the undeformed configuration. Plastic strains at the smoothly blunted surface of an originally sharp crack are infinite and this leads to infinite flow stresses there in power law hardening materials. However the large stresses are confined to a small volume of material typically well within 0.1 crack tip openings from the blunted surface in the deformed configuration, for hardening levels typical of structural metals. In addition to the distribution of stress and deformation near the tip, a relationship

between the applied load and crack tip opening displacement for small scale yielding was established. It was shown that the J-integral is path dependent except in an area very close to the crack tip, where the calculations indicate that a path dependence arises.

The results of the finite element solutions confirm that the slip line approach of RICE and JOHNSON (1970) models the essential crack blunting behavior for elastic-non-hardening plastic materials, and that the extension of the results for stress to hardening materials in their work is a fairly accurate approximation.

The stress and strain fields calculated by finite elements have been applied to criteria and models for initiation of crack growth. In the absence of fully worked out models for this event, few definitive comments can be made. But the implications of some partially formulated models are clear. In particular, calculations using models for void growth near the crack tip can lead to useful results, but more general application of these awaits the development of criteria for void nucleation and the improvement of models for void-crack and void-void coalescence. The topography of observed crack growth initiation in small scale yielding can be used along with the results for near tip stress and plastic strain to deduce the importance of stress or strain in the fracture model. For example, straight ahead growth might suggest a stress controlled process while angled crack growth seems to suggest a plastic strain dominated process. In consequence, extensive work in sectioning propped open blunted cracks in small scale yielding prior to and immediately following ductile crack extension would seem to be in order, to assess the value of the various fracture criteria and void growth models discussed.

ACKNOWLEDGEMENT

This study was supported by the Energy Research and Development Administration under Grant E(11-1)-3084. I wish to thank Dr. P. V. Marcal for provision of the MARC program and Dr. D. K. Brown for helping with the computations. In addition, the many helpful discussions with Professors J. R. Rice and D. M. Parks are gratefully acknowledged.

REFERENCES

ARGON, A. S., and IM, J.	1975	Met. Trans. 6A, 839.
ASHBY, M. F.	1966	Phil. Mag. 14, 1157.
BATES, R. C., and CLARK, W. G.	1969	Trans. Am. Soc. Metals 62,380.
BEACHEM, C. D., and YODER, G. R.	1973	Met. Trans. 4, 1145.
BERG, C. A.	1970	Inelastic Behavior of Solids (Edited by KANNINEN, M. F., ADLER, W. F., ROSENFIELD, A. R., and JAFFEE, R. I.) p. 171 McGraw-Hill, New York.
BIRKLE, A. J., WEI, R. P., and PELLISSIER, G. E.	1966	Trans. Am. Soc. Metals 59,981.
BLUHM, J. I., and MORRISEY, R. J.	1966	Proceedings of the 1st International Conference on Fracture,(Edited by YOKOBORI, T., KAWASAKI, T., and SWEDLOW, J. L.) Vol. 3, Japanese Society for Strength and Fracture of Materials.
BROEK, D.	1974	Engg. Fracture Mech. 6, 173.
BROTHERS, A. J., HILL, M., PARKER, M. T., SPITZIG, W. A., WIEBE, W., and WOLFF, U. E.	1971	A.S.T.M., S.T.P. 493, p. 3.
CLAUSING, D. P.	1970	Int. J. Fracture Mech. 6,71.
CLAYTON, J. Q., and KNOTT, J. F.	1976	Metal Sci. 10, 63.
COX, T. B., and LOW, J. R.	1974	Met. Trans. 5, 1457.
GREEN, G., and KNOTT, J. F.	1976	Trans. A.S.M.E.(Series H,J. Engg. Mat. Tech.) 98,37.
GREEN, G., SMITH, R. F., and KNOTT, J. F.	1973	Proceedings of B.S.C. Conference on Mechanics and Mechanisms of Crack Growth (Cambridge, April 1973)(Edited by MAY, M.J.) paper 5. British Steel Corporation, London.
GURLAND, J.	1963	Trans. Metall. Soc. A.I.M.E. 227, 1146.
GURLAND, J., and PLATEAU, J.	1963	Trans. Am. Soc. Metals 56, 442.

HAHN, G. T., and ROSENFIELD, A. R.	1975	Met. Trans. 6A, 653.
HAYES, D. J., and TURNER, C. E.	1974	Int. J. Fracture 10, 17.
HILL, R.	1950	The Mathematical Theory of Plasticity, Oxford University Press, London.
	1959	J. Mech. Phys. Solids 7, 209.
	1962	Ibid., 10, 1.
	1967	Ibid., 15, 255.
HUFF, H. W., JOYCE, J. A., and McCLINTOCK, F. A.	1969	Fracture 1969 (Proceedings of the 2nd International Conference on Fracture, Brighton, April 1969), (Edited by PRATT, P.L.) p. 83, Chapman and Hall, London.
HUTCHINSON, J. W.	1968	J. Mech. Phys. Solids 16, 13.
	1970	Proc. Roy. Soc. Lond. A319, 247.
IRWIN, G. R.	1960	Structural Mechanics (Edited by GOODIER, N. J. et al) p. 557, Pergamon Press, London.
KOBAYASHI, A. S., CHIU, S.T., and BEEUWKES, R.	1973	Engg. Fracture Mech. 5, 293.
KRAFFT, J. M.	1964	Appl. Mat. Res. 3, 88.
MACKENZIE, A. C., HANCOCK, J. W., and BROWN, D. K.	1973	Final Report, Fracture Group (Contract N/CP 75/52069/SC538), Mechanical Engineering, University of Glasgow.
MARCAL, P. V., and KING, I. P.	1967	Int. J. Mech. Sci. 9, 143.
McCLINTOCK, F. A.	1958	J. Appl. Mech. 25, 582.
	1968a	Ibid., 35, 363.
	1968b	Ductility (Edited by PAXTON, H. W.) p. 255, American Society for Metals, Metals Park, Ohio.
	1971	Fracture, An Advanced Treatise (Edited by by LIEBOWITZ, H.) Vol. 3, p. 47. Academic Press, New York.
McMEEKING, R. M.	1976	Ph.D. Dissertation, Brown University.
McMEEKING, R. M., and RICE, J. R.	1975	Int. J. Solids Structures 11, 601.

NAGTEGAAL, J. L., PARKS, D. M., and RICE, J. R.	1974	Comp. Methods Appl. Mech. Engg. 4, 153.
OSBORNE, D. E., and EMBURY, J. D.	1973	Met. Trans. 4, 2051.
PARKS, D. M.	1975	Ph.D. Dissertation, Brown University.
	1976	Trans. A.S.M.E. (Series H, J. Engg. Mat. Tech.) 98, 30.
PELLISSIER, G. E.	1968	Engg. Fracture Mech. 1, 55.
PSIODA, J. A., and LOW, J. R.	1974	Carnegie-Mellon University Technical Report NASA 6/NGR 39-087-003.
RAWAL, S. P., and GURLAND, J.	1976	Proceedings of 2nd International Conference on Mechanical Behavior of Materials (Boston, August 1976), in press; also Brown University Technical Report E(11-1)-3084/41.
RICE, J. R.	1967a	A.S.T.M., S.T.P. 415, p. 247.
	1967b	J. Appl. Mech. 34, 287.
	1968	Ibid., 35, 379.
	1973	Proceedings of 3rd International Congress on Fracture, Vol. II, paper I-441, Verein Deutscher Eisenhuettenleute, Dusseldorf.
	1976	Proceedings of 14th International Congress of Theoretical and Applied Mechanics, Vol.I, North-Holland, (in press).
RICE, J. R. and JOHNSON, M. A.	1970	Inelastic Behavior of Solids (Edited by KANNINEN, M. F., ADLER, W. F., ROSENFIELD, A. R., and JAFFEE, R. I.) p. 641 McGraw-Hill, New York.
RICE, J. R., and ROSENGREN, G. F.	1968	J. Mech. Phys. Solids 16, 1.
RICE, J. R., and TRACEY, D. M.	1969	Ibid., 17, 201.
	1973	Numerical and Computer Methods in Structural Mechanics (Edited by FENVES, S. J. et al) p. 585, Academic Press, New York.
RITCHIE, R. O., KNOTT, J. F., and RICE, J. R.	1973	J. Mech. Phys. Solids 21, 395.
ROBINSON, J. N., and TETELMAN, A. S.	1974	A.S.T.M., S.T.P., 559,p.139.

ROGERS, H. C.	1960	Trans. Metall. Soc. A.I.M.E. 218, 498.
TANAKA, K., MORI, T., and NAKAMURA, T.	1971	Phil. Mag. 21, 267.
TRACEY, D. M.	1973	Ph.D. Dissertation, Brown University
	1976	Trans. A.S.M.E. (Series H, J. Engg. Mat. Tech) 98, 146.
VAN DEN AVYLE, J. A.	1975	Ph.D. Dissertation, Massachusetts Institute of Technology.
VAN STONE, R. H., MERCHANT, R. H., and LOW, J. R.	1974	A.S.T.M.,S.T.P. 556, p. 93.
VAN STONE, R. H., and PSIODA, J. A.	1975	Met. Trans. 6A, 668.
ZIENKIEWICZ, O. C.	1971	The Finite Element Method in Engineering Science, McGraw-Hill, London.

TABLE CAPTION

Relation between crack tip opening displacement δ_t and applied load as parameterized by J_{app}/σ_o for four materials inferred from finite element results using various definitions of notch width as follows: I - as in fig. 8, based on point A'; II - notch width defined at point of intersection of the notch surface and a line drawn at 45° to the x axis, from the intersection of the notch tip and the x-axis; III - notch width defined at the elastic-plastic boundary.

Table

σ_o	N	n as in $\delta_t = nJ_{app}/\sigma_o$		
		I	II	III
1/300	0	0.55	0.58	0.61
1/300	0.1	0.41	0.44	0.60
1/300	0.2	0.27	0.30	0.54
1/100	0	0.67	0.65	0.63

LIST OF FIGURE CAPTIONS

Figure 1. Undeformed configuration of finite element mesh I for the notch blunting solution.

Figure 2. (a) Shapes of the blunted notches calculated by finite elements and by the slip line method.

(b) Estimates of blunted crack tip shape inferred from finite element calculations and the shape for a sharp crack deduced by slip line method.

Figure 3. Plot of stress $\sigma_{\theta\theta}/\sigma_o$ and plastic strain around the blunted notch for $\sigma_o/E = 1/300$ and $N = 0$. Note σ_o is the yield stress in tension and R and θ are defined for the position of the material in the undeformed configuration.

Figure 4. Plot of stress $\sigma_{\theta\theta}/\sigma_o$ and plastic strain around the blunted notch for $\sigma_o/E = 1/300$ and $N = 0.1$.

Figure 5. Plot of stress $\sigma_{\theta\theta}/\sigma_o$ and plastic strain around the blunted notch for $\sigma_o/E = 1/300$ and $N = 0.2$.

Figure 6. Plot of stress $\sigma_{\theta\theta}/\sigma_o$ and plastic strain around the blunted notch for $\sigma_o/E = 1/100$ and $N = 0$.

Figure 7. Plot of stress σ_{yy}/σ_o on crack line ($\theta = 0$) versus distance from crack tip in undeformed configuration from slip line solution and approximation of RJ.

Figure 8. Plot of notch width b versus the value of the J-integral, J_{app}, computed on a remote contour around the notch tip.

Figure 9. Plot of J-integral, computed as a contour integral, versus distance of contour from the notch tip.

Figure 10. Slip line fields around crack tips blunted to shapes with corners.

Figure 11. Plot of dimensions of a void growing in the near tip field in the material $\sigma_o/E = 1/300$, N = 0 versus the notch width. The void starts growing as soon as it enters the plastic zone.

Figure 12. Plot of dimensions of void growing in near tip field in material $\sigma_o/E = 1/300$, N = 0.1. versus notch width.

Figure 13. Data for crack tip opening displacement at initiation of crack growth or fracture, related to particle spacing D and particle size a_o. Also criterion for fracture as formulated by RJ.

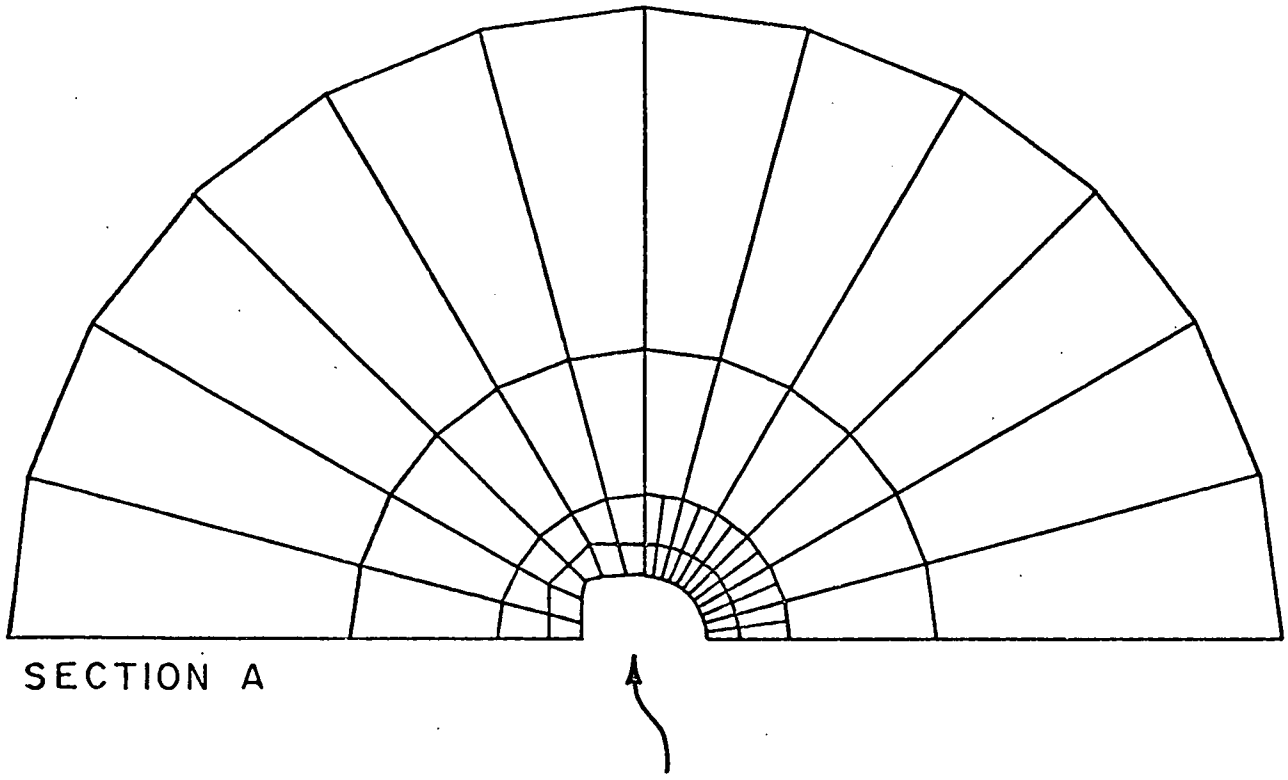

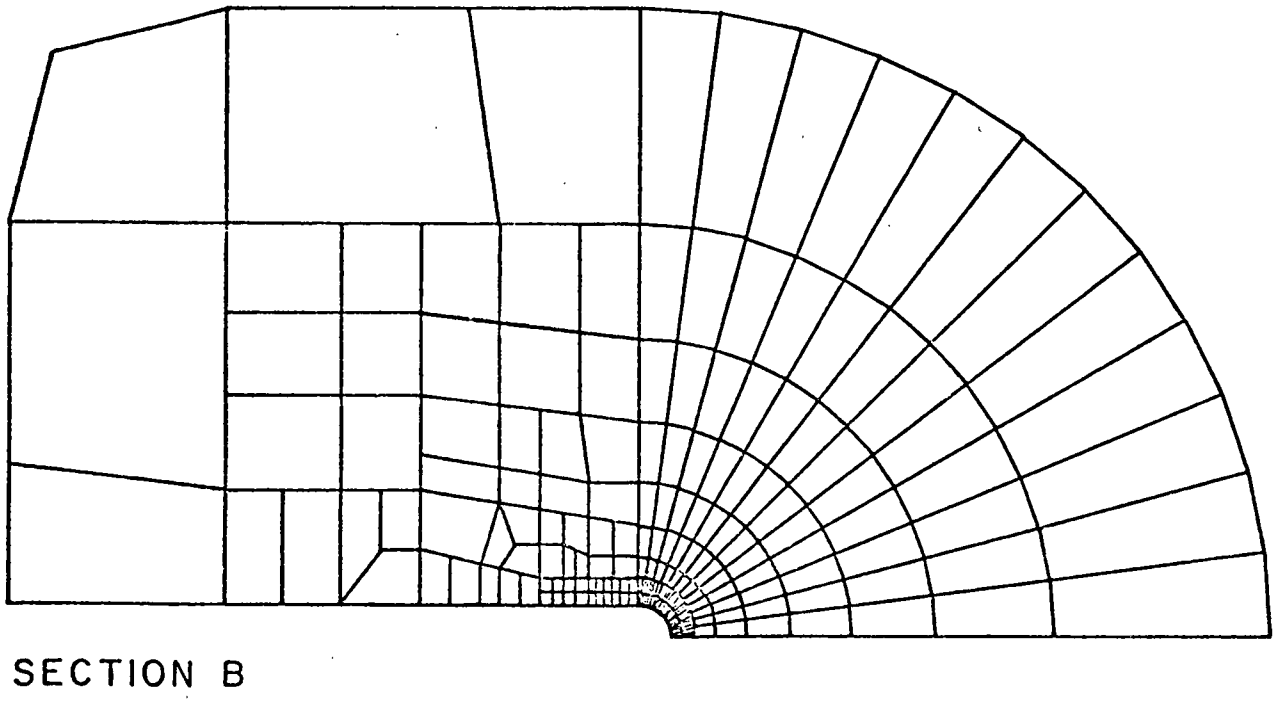

FIGURE 1

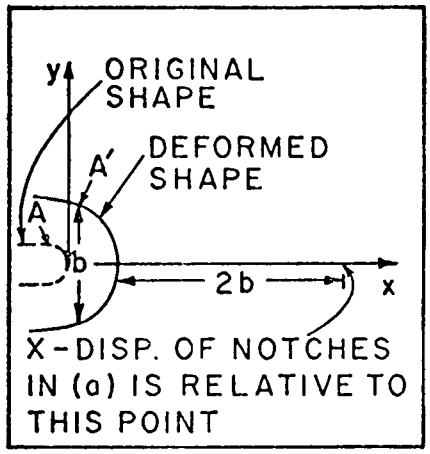

FINITE ELEMENT RESULTS

..... N=0
----- N=0.1
—·—·— N=0.2

$\frac{\sigma_0}{E} = \frac{1}{300}$

...-...- N=0 $\frac{\sigma_0}{E} = \frac{1}{100}$

SLIP LINE RESULTS

——— RICE & JOHNSON (1970)

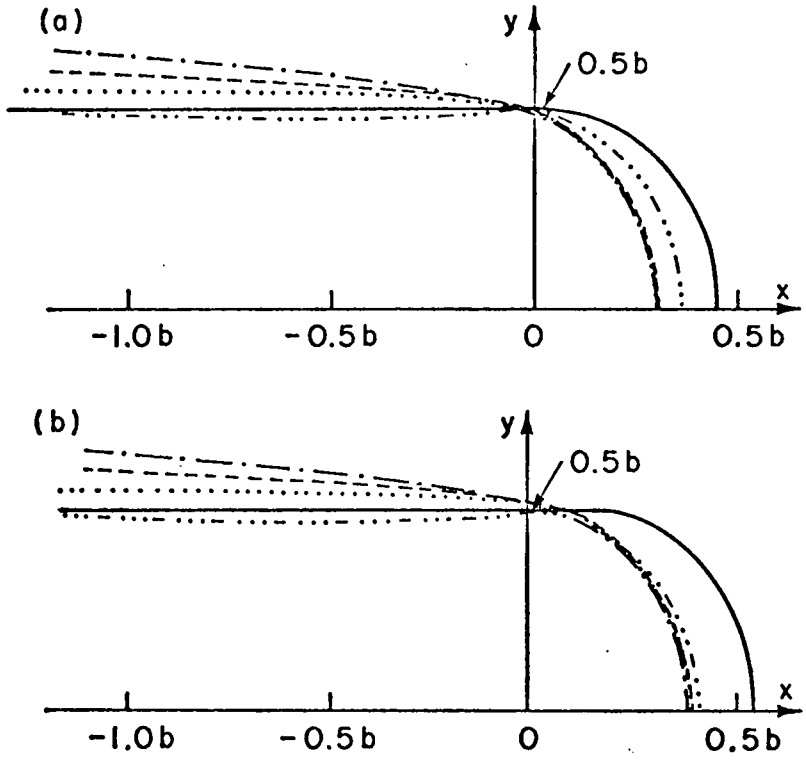

FIGURE 2

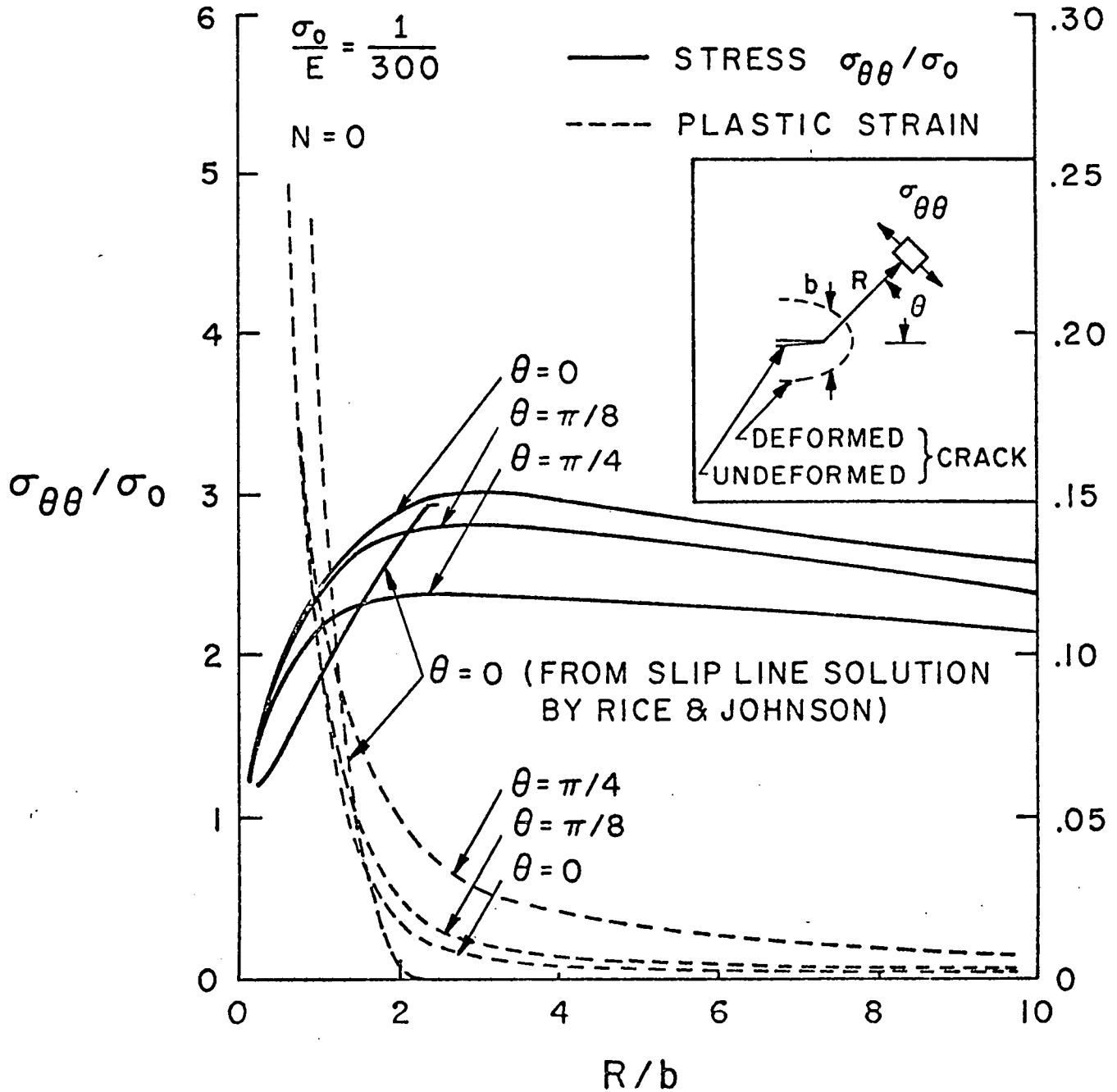
$\frac{\sigma_0}{E} = \frac{1}{300}$
N = 0
STRESS $\sigma_{\theta\theta}/\sigma_0$
PLASTIC STRAIN
$\sigma_{\theta\theta}$
b
R
θ
DEFORMED
UNDEFORMED
CRACK
$\theta = 0$
$\theta = \pi/8$
$\theta = \pi/4$
$\theta = 0$ (FROM SLIP LINE SOLUTION BY RICE & JOHNSON)
$\theta = \pi/4$
$\theta = \pi/8$
$\theta = 0$
$\sigma_{\theta\theta}/\sigma_0$
ϵ^p
R/b
0
1
2
3
4
5
6
0
2
4
6
8
10
.30
.25
.20
.15
.10
.05
0

FIGURE 3

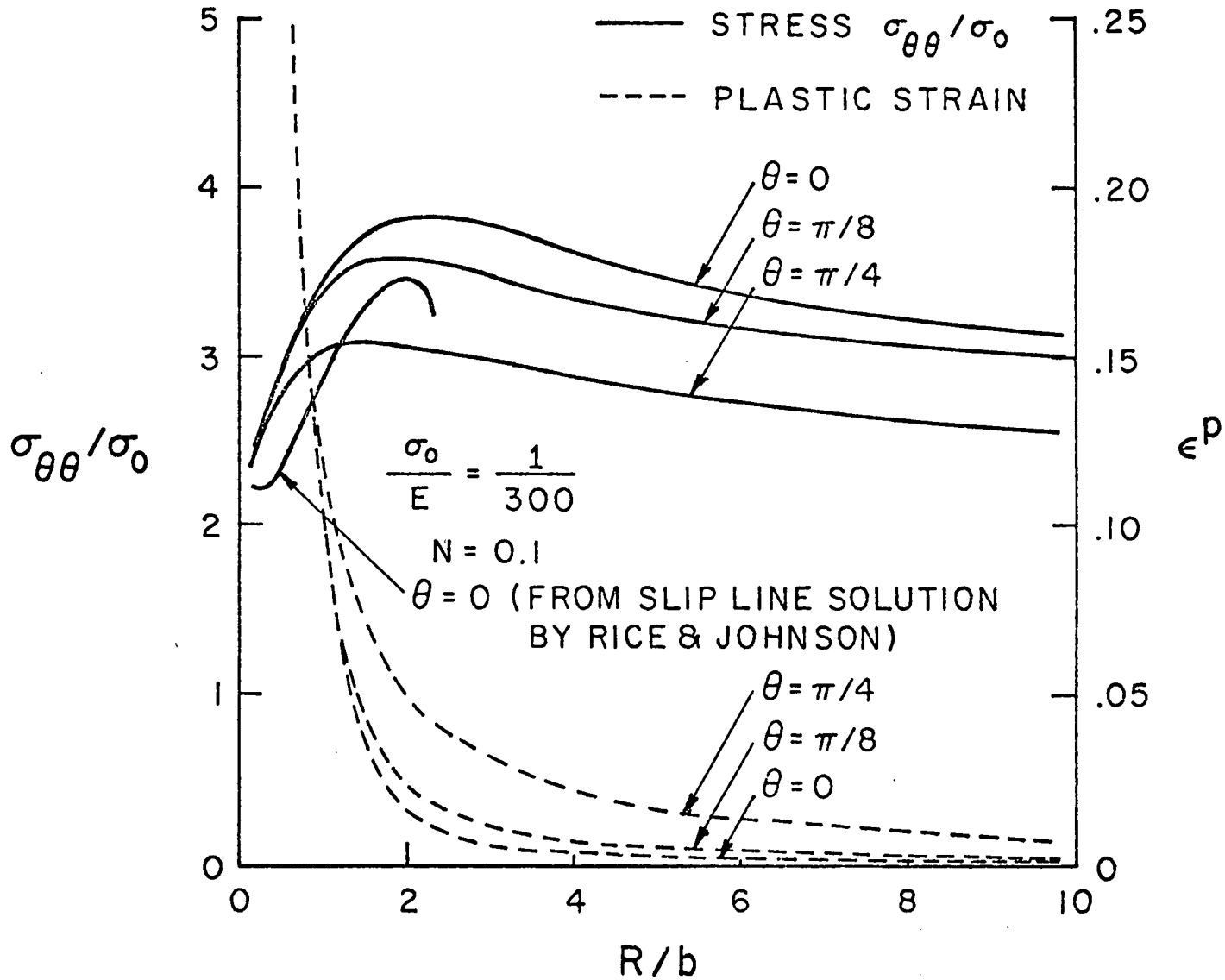
STRESS $\sigma_{\theta\theta}/\sigma_0$
PLASTIC STRAIN
$\theta = 0$
$\theta = \pi/8$
$\theta = \pi/4$
$\frac{\sigma_0}{E} = \frac{1}{300}$
N = 0.1
$\theta = 0$ (FROM SLIP LINE SOLUTION BY RICE & JOHNSON)
$\theta = \pi/4$
$\theta = \pi/8$
$\theta = 0$
$\sigma_{\theta\theta}/\sigma_0$
ϵ^p
R/b
0
1
2
3
4
5
.05
.10
.15
.20
.25
0
2
4
6
8
10

FIGURE 4

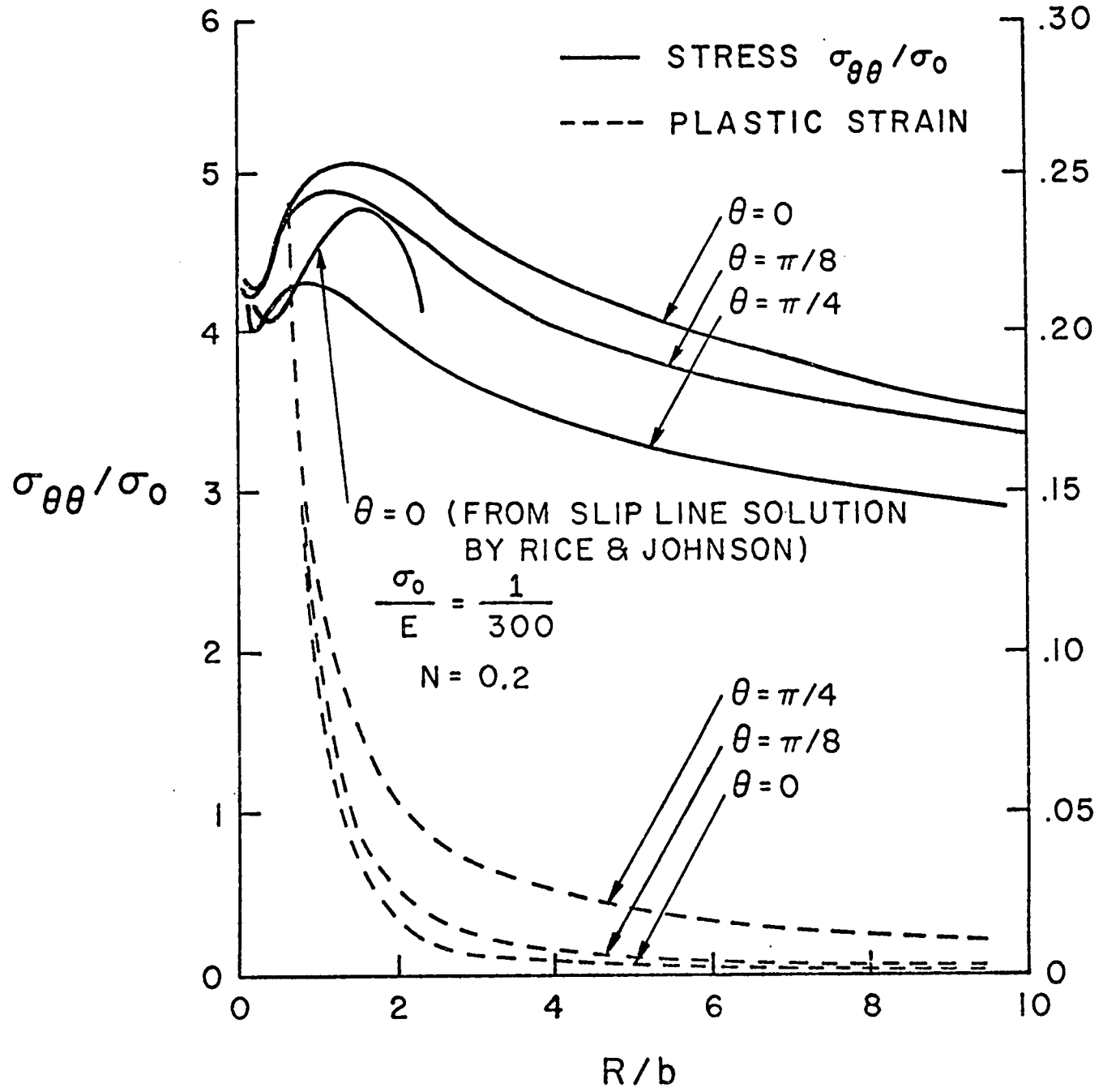
STRESS $\sigma_{\theta\theta}/\sigma_0$
PLASTIC STRAIN
$\theta = 0$
$\theta = \pi/8$
$\theta = \pi/4$
$\theta = 0$ (FROM SLIP LINE SOLUTION BY RICE & JOHNSON)
$\frac{\sigma_0}{E} = \frac{1}{300}$
N = 0.2
$\theta = \pi/4$
$\theta = \pi/8$
$\theta = 0$
$\sigma_{\theta\theta}/\sigma_0$
ϵ^p
R/b
0
1
2
3
4
5
6
.05
.10
.15
.20
.25
.30
0
2
4
6
8
10

FIGURE 5

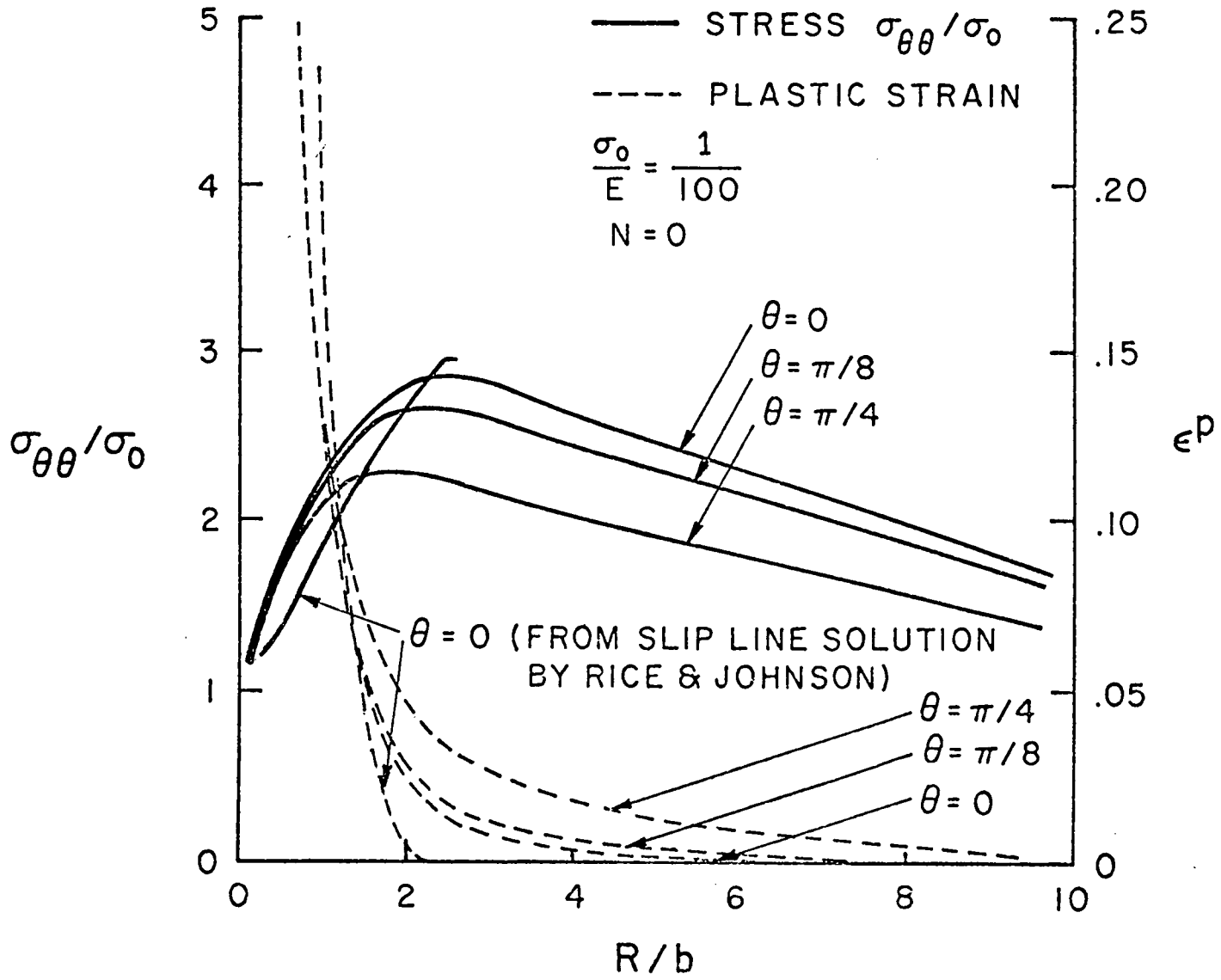
STRESS $\sigma_{\theta\theta}/\sigma_0$
PLASTIC STRAIN
$\frac{\sigma_0}{E} = \frac{1}{100}$
N = 0
$\theta = 0$
$\theta = \pi/8$
$\theta = \pi/4$
$\theta = 0$ (FROM SLIP LINE SOLUTION BY RICE & JOHNSON)
$\theta = \pi/4$
$\theta = \pi/8$
$\theta = 0$
$\sigma_{\theta\theta}/\sigma_0$
ϵ^p
R/b
0
1
2
3
4
5
0
2
4
6
8
10
.05
.10
.15
.20
.25

FIGURE 6

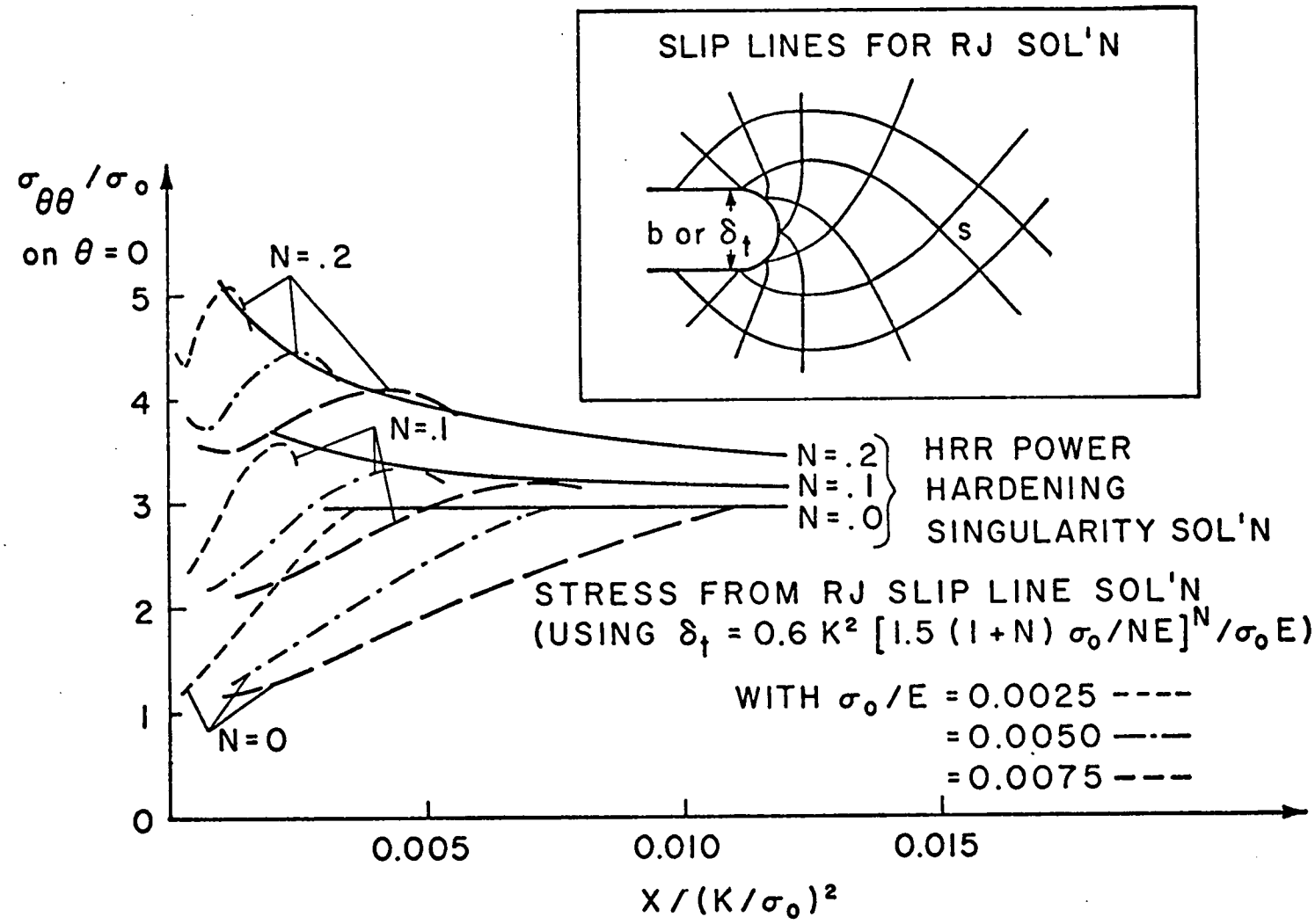
SLIP LINES FOR RJ SOL'N
b or δ_t
s
$\sigma_{\theta\theta}/\sigma_o$
on $\theta = 0$
N=.2
N=.1
N=0
N=.2
N=.1
N=.0
HRR POWER
HARDENING
SINGULARITY SOL'N
STRESS FROM RJ SLIP LINE SOL'N
(USING $\delta_t = 0.6\,K^2\,[1.5\,(1+N)\,\sigma_o/NE]^N/\sigma_o E$)
WITH σ_o/E = 0.0025 ----
= 0.0050 —·—
= 0.0075 — — —
0
1
2
3
4
5
0.005
0.010
0.015
$X/(K/\sigma_o)^2$

FIGURE 7

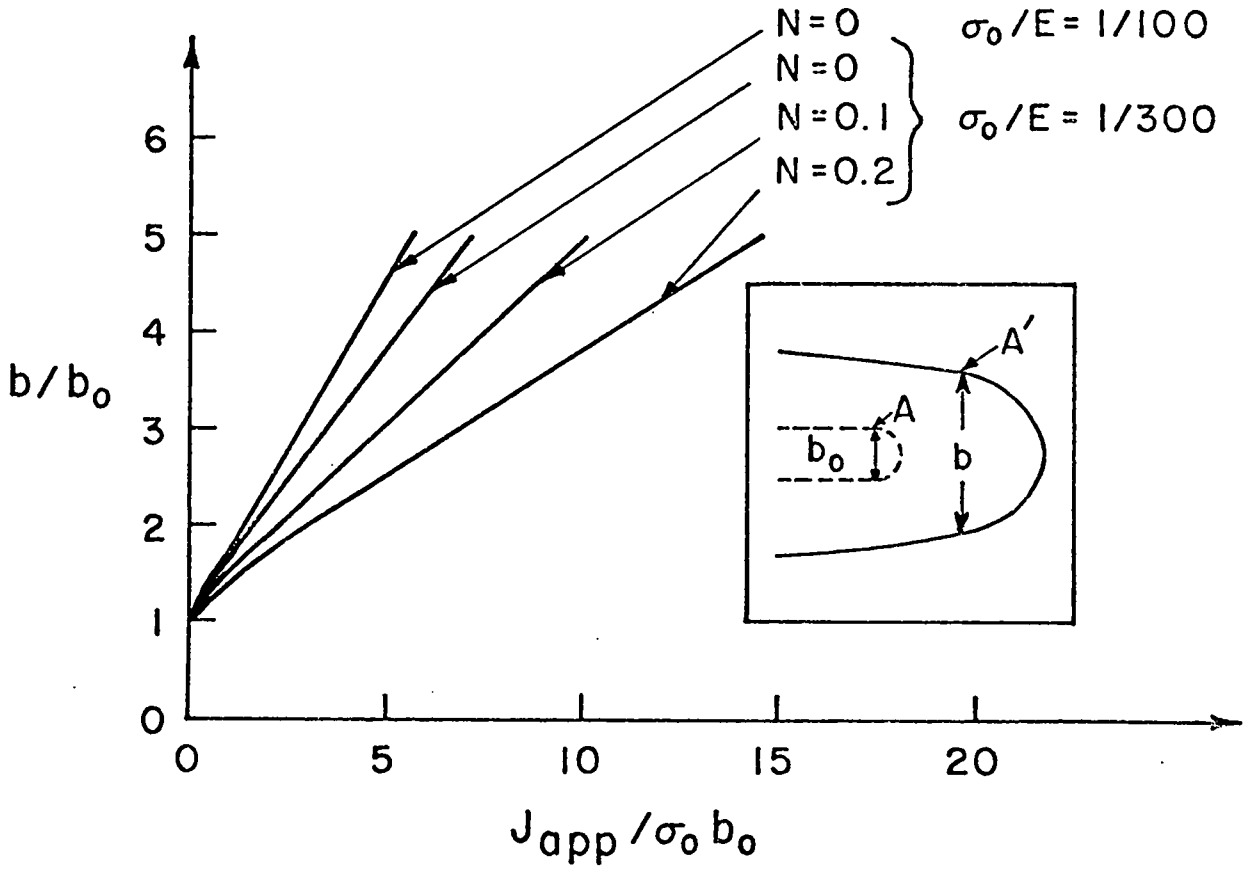
N = 0
N = 0
N = 0.1
N = 0.2
σ0/E = 1/100
σ0/E = 1/300
A'
A
b0
b
b/b0
0
1
2
3
4
5
6
0
5
10
15
20
Japp/σ0 b0

FIGURE 8

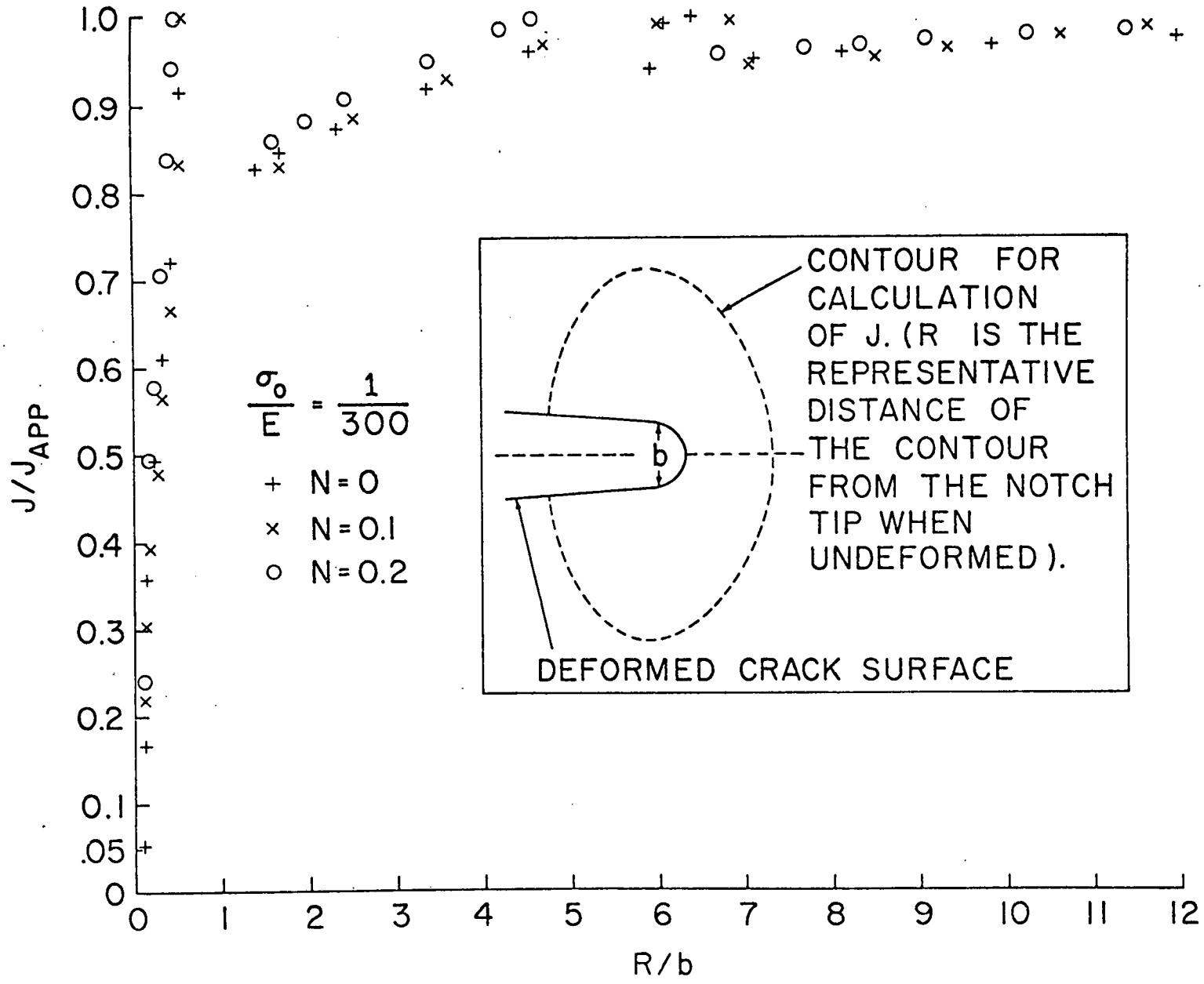
1.0
0.9
0.8
0.7
0.6
0.5
0.4
0.3
0.2
0.1
.05
0
J/J_APP
0
1
2
3
4
5
6
7
8
9
10
11
12
R/b
σ0/E = 1/300
+ N=0
× N=0.1
○ N=0.2
b
CONTOUR FOR CALCULATION OF J. (R IS THE REPRESENTATIVE DISTANCE OF THE CONTOUR FROM THE NOTCH TIP WHEN UNDEFORMED).
DEFORMED CRACK SURFACE

FIGURE 9

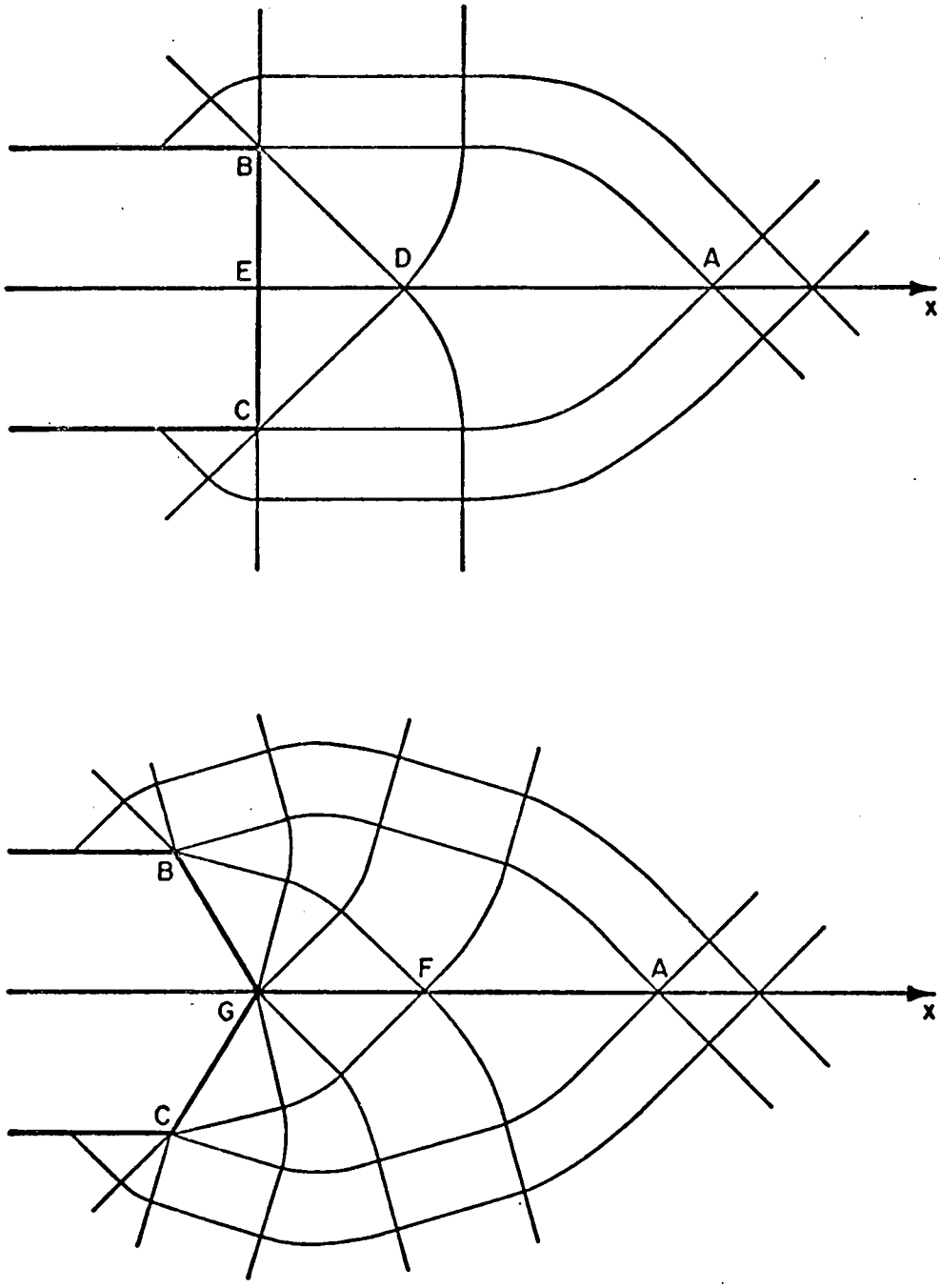

FIGURE 10

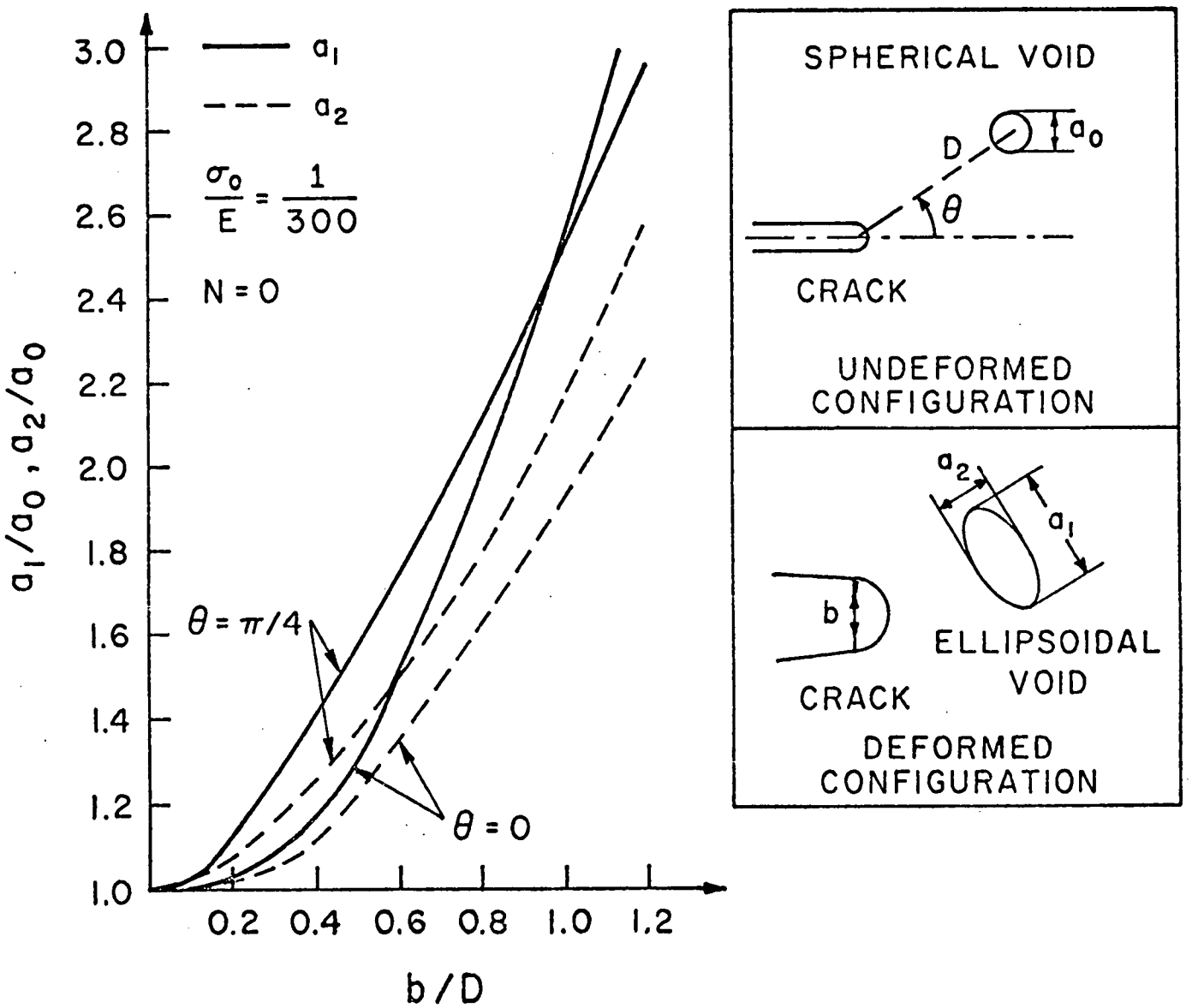
3.0
2.8
2.6
2.4
2.2
2.0
1.8
1.6
1.4
1.2
1.0
a_1/a_0 , a_2/a_0
a_1
a_2
$\frac{\sigma_0}{E} = \frac{1}{300}$
N = 0
$\theta = \pi/4$
$\theta = 0$
0.2 0.4 0.6 0.8 1.0 1.2
b/D
SPHERICAL VOID
D
a_0
θ
CRACK
UNDEFORMED CONFIGURATION
a_2
a_1
b
CRACK
ELLIPSOIDAL VOID
DEFORMED CONFIGURATION

FIGURE 11

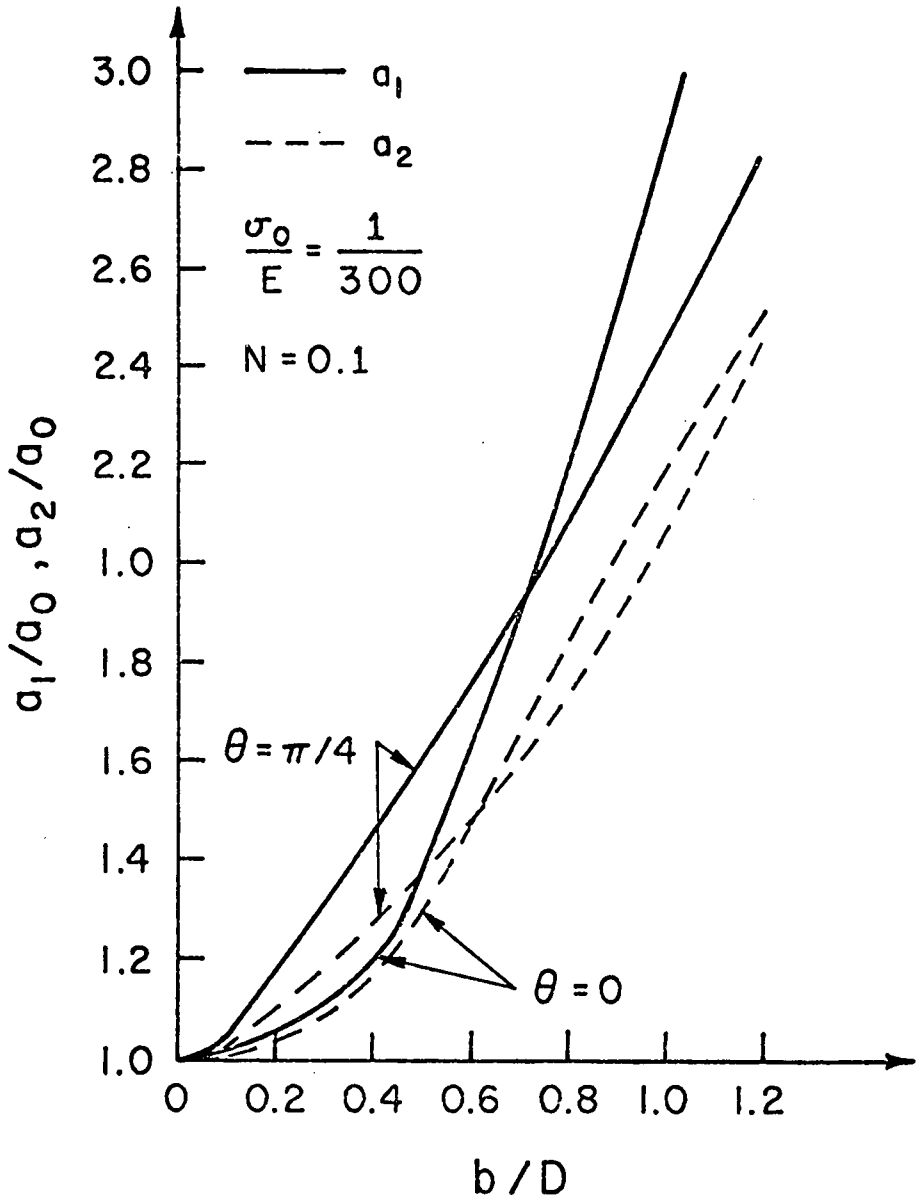
3.0
2.8
2.6
2.4
2.2
1.0
1.8
1.6
1.4
1.2
1.0
a_1
a_2
$\frac{\sigma_0}{E} = \frac{1}{300}$
N = 0.1
$\theta = \pi/4$
$\theta = 0$
a_1/a_0 , a_2/a_0
0
0.2
0.4
0.6
0.8
1.0
1.2
b / D

FIGURE 12

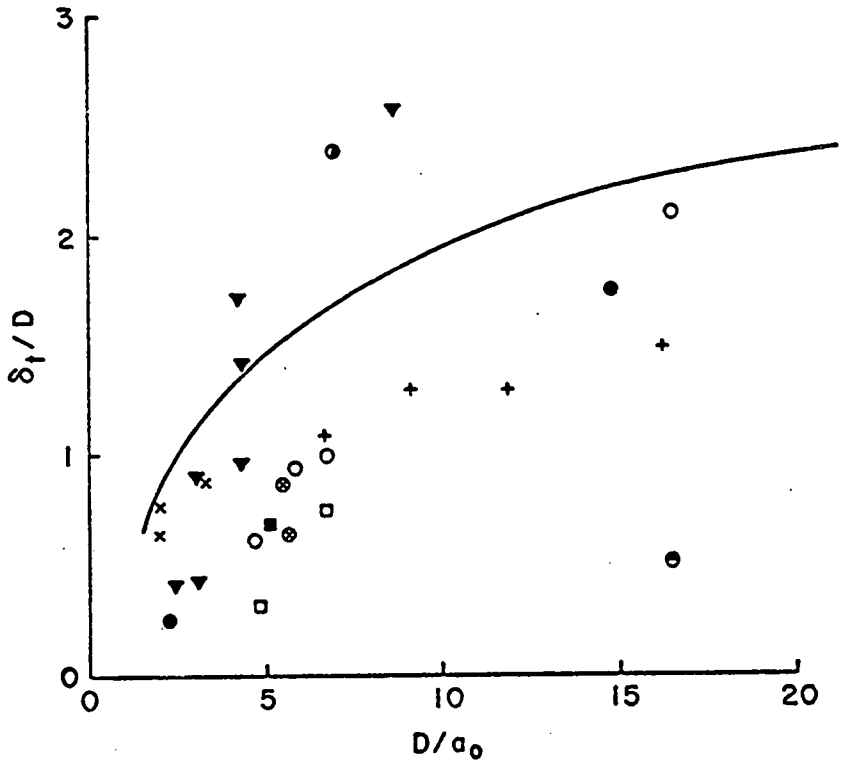

DATA FROM FRACTURE TOUGHNESS TESTS

+ HIGH STRENGTH STEEL (MnS INCLUSIONS), RICE & JOHNSON (1970), PELLISSIER (1968)

× ALUMINUM 2000 SERIES } VAN STONE
⊗ ALUMINUM 7000 SERIES } ET AL (1974), RICE

□ AISI 4340 STEEL (MnS INCLUSIONS) } COX & LOW (1974)
■ 18-Ni. 200 MARAGING STEEL (T_i(C,N) INCLUSIONS) } COX & LOW (1974)

▼ MILD STEEL (SPHEROIDIZED Fe_3C INCLUSIONS), RAWAL & GURLAND (1976)

DATA FROM CRACK GROWTH INITIATION TESTS

○ ENIA MILD STEEL
◒ PRESTRAINED ENIA
◐ ENIA (LONGITUDINAL SPECIMEN)
● C/Mn STEEL
} GREEN & KNOTT (1976)

FRACTURE MODEL

— SMALL SCALE YIELDING, RICE & JOHNSON (1970)

FIGURE 13